東京大学大学院新領域創成科学研究科

基盤科学研究系

先端エネルギー工学専攻

平成21年度

修士論文

Thermodynamic model of the turbulent heat transport in plasma boundary layer: Bifurcation, stability and hysteresis

—プラズマ境界層における乱流熱輸送の熱力学モデル： 分岐現象，安定性とヒステリシス—

2010年2月提出

指導教員　吉田　善章　教授

47086063　川面　洋平

ABSTRACT

The aim of this study is to analyze the underlying thermodynamic relations governing the self-organization in turbulent fluid/plasma systems. Many of the turbulent systems are open non-equilibrium systems from the macroscopic point of view. The debate on the entropy production rate has not been settled over; the "minimum entropy production rate principle" is known to be widely applicable to characterizing the self-organized structures in non-equilibrium thermodynamic systems, but is often disproved by the observations of "maximum entropy production rate states". Here we reveal a "dual" relation between the minimum and maximum principles; the mathematical representation of the duality is given by a Legendre transformation. We study a phenomenological model of heat transport in the boundary layer of fusion plasma. The mechanism of hysteresis (which is characteristic determining of the bifurcation of the so-called H-mode, a self-organized state of reduced thermal conduction) is explained by the tangent line problem. Taking the neoclassical theory of H-mode for example, this phenomenological model is proved to be connected

smoothly to the realistic theory.

Contents

List of Figures

Chapter 1

Introduction

1.1 Background

Self-organization phenomena, such as the formation of a zonal flow in planet's atmosphere[1] or tokamak plasma[2], occurs in various turbulent fluid or plasma systems. To describe these, inherent mechanisms for each phenomena cannot help being considered individually. On the other hand, these are non-equilibrium open thermodynamic systems from a macroscopic point of view. All kinds of the phenomena are expected to be explained by thermodynamics – any physical system cannot violate thermodynamic law –. In thermodynamics, seeking variational or extremization principles is often quite fruitful;

The principle of maximum entropy and the principle of minimum free energy are the examples in equilibrium thermodynamics. Well-known equilibrium thermodynamics using entropy, however, may not explain non-equilibrium phenomena. The entropy production rate (EP) is deemed capable of dictating "self-organized structures" in non-equilibrium thermodynamic (or macroscopic) systems (Remembering equation of motion in dynamics, breaking the balance of power induces acceleration (change "rate" of velocity)). There are two seemingly opposing variational principles about entropy production rate – the principle of maximum entropy production rate and the principle of minimum entropy production rate –.

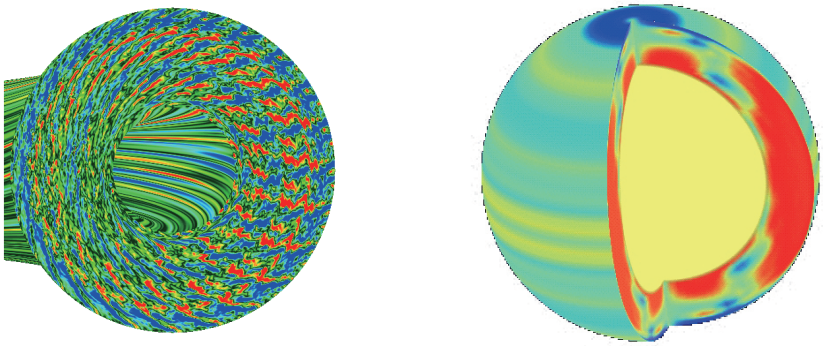

Figure 1.1: Typical examples of zonal flow[3]

Prigogine[4] and the collaborators found that many of structures (heterogeneous distributions of physical quantities), which emerge and sustain in non-equilibrium thermodynamic systems, are characterized as the minimizers of some appropriately defined entropy production rates. This "minimum entropy production rate principle" is certainly a natural extension of Dirichlet's principle of the linear diffusion equation to some class of nonlinear dissipative systems (primarily the reaction-diffusion equations).

However, the minimum principle is not universal; Paltridege[5] found that, in the heat transfer through the planet's atmosphere, the temperature contrast between the tropical region and the polar regions tends to be maximized, thus the entropy production rate (= heat flux multiple of the temperature contrast) prefers the maximum. The maximization of temperature gradient between warm tropics and cool region is also found in other planets too[9]. Ozawa *et al.* proposed that these maximization of entropy production rate is caused by fluid mechanical instabilities[10]. Dewar proposed statistical mechanics theory possibly explaining maximum entropy production in non-equilibrium systems using Jaynes formalism[11, 12]. Yoshida & Mahajan[13] pointed out that a "flux-driven system" tends to maximize the entropy production rate. A simple example of flux-driven systems can be composed by connecting a

(nonlinear) impedance (Z) to a constant-current (I) power supply, which is compared with a "force-driven" counterpart composed of the impedance and a constant-voltage (V) power supply. In the former case the entropy production rate is ZI^2, while in the latter case it is V^2/Z. If the nonlinear impedance has bifurcated operation points, and the system selects the largest value of Z, the constant-current (flux-driven) system maximizes the entropy production rate, while the constant-voltage (force-driven) system minimizes the entropy production rate. In this paper, we shall formulate the mini-max duality of the entropy production rate (or relation between the flux-driven and force-driven systems) as a Legendre transformation.

As previously mentioned, a turbulent fluid system tends to maximize the entropy production rate. Yoshida & Mahajan explained the reason by formulating a flux-driven model of turbulent heat transport (to be reviewed and extended in Chapter 2). How energy flux drives turbulence is always the central issue of turbulence theories; for example, Kolmogorov's model of energy cascade is derived by the dimensional analysis of the energy flux (injection rate = transfer rate = dissipation rate), energy spectrum density, wave number, and the kinematic viscosity.

1.2 Variational principle of entropy production rate

The entropy production rate without mass flow is exactly written as a volume integral of the inner product of heat flow $\boldsymbol{f}$ and thermodynamic power $\nabla(1/T)$[14, 15] (see Appendix A).

$$\dot{S} = \int_V \boldsymbol{f} \cdot \nabla \left(\frac{1}{T} \right) d^3x \tag{1.1}$$

In general, diffusive process without flow is thought to be explained by "minimum entropy production rate". Since Fick's law is kept in this "quasi linear state", irreversible flow is written as $\boldsymbol{f} = -D\nabla T$. Then entropy production rate is,

$$\begin{aligned} \dot{S} &= \int_V -D\nabla T \cdot \nabla \left(\frac{1}{T} \right) d^3x = \int_V D \left(\frac{\nabla T}{T} \right)^2 d^3x \\ &= \int_V D(\nabla \ln T)^2 d^3x \end{aligned} \tag{1.2}$$

Now we prove $\dot{S}$ is saturated in minimum in the final state of time evolution. Time variation of $\dot{S}$, defining $U \equiv \ln T$, is calculated as,

$$\begin{aligned}\frac{d}{dt}\dot{S} &= 2D\int_V \nabla U\cdot\frac{\partial}{\partial t}\nabla U d^3x \\ &= 2D\left[\int_V \nabla U\cdot\left(\nabla\frac{\partial U}{\partial t}\right)d^3x - \int_V \nabla^2 U\frac{\partial U}{\partial t}d^3x\right]\end{aligned} \tag{1.3}$$

The second term of the right hand side equals zero by Gauss's law and boundary condition $\partial U/\partial t = 0$ on ∂V. Energy conservation law without mass flow is,

$$\frac{\partial}{\partial t}(\rho u) + \nabla\cdot\boldsymbol{f} = 0 \tag{1.4}$$

where u is internal energy. Heat capacity at constant volume is defined as $C_V = \partial U/\partial T$. Therefore we obtain the change rate of T as,

$$C_V\frac{\partial T}{\partial t} = \frac{\partial}{\partial t}(\rho u) \tag{1.5}$$

From equation (1.4) and (1.5) we obtain following relation.

$$C_V\frac{\partial T}{\partial t} = D\nabla^2 T \tag{1.6}$$

Dividing both side by T we obtain,

$$C_V\frac{\partial U}{\partial t} = D\nabla^2 U \tag{1.7}$$

Substituting this into equation (1.3),

$$\frac{d}{dt}\dot{S} = -2C_V \int_V \left(\frac{\partial U}{\partial t}\right)^2 d^3x < 0 \tag{1.8}$$

The entropy production rate decreases as time goes by. Then the final condition is realized as the minimum of entropy production.

Next, tangible profile of temperature shall be found out. To obtain the extremum of Temperature field $T(\boldsymbol{x})$, the variation $\delta[F(U, \nabla U, \boldsymbol{x})] = 0$ is calculated where $F(U, \nabla U, \boldsymbol{x}) \equiv (\nabla U)^2$.

From Euler-Lagrange equation

$$\frac{\partial F}{\partial U} - \nabla \cdot \frac{\partial F}{\partial(\nabla U)} = 0 \tag{1.9}$$

the solution is $\nabla^2 \ln T = 0$ ($\nabla^2 U = 0$). That is to say, if we assume the system as one dimensional, temperature field profile is $T(x) = T_0 \exp[x \ln(T_1/T_0)/L]$ with boundary condition $T(0) = T_0$, $T(L) = T_1$.

This differs from Fourier's law that is deemed to be holding in the linear diffusion state. Under the assumption of small temperature gradient ($\nabla T/T \simeq k\nabla T$), entropy production rate (1.2) turns into $\kappa \int_V (\nabla T)^2 d^3x$. Though variation of approximated entropy production rate yields the Fourier's law, this is not strict.

Above discussion is predicated on linear relation between flow and thermodynamic power. In these words, minimum entropy production is obvious only in a state as the linear relation holds. When we consider systems far from equilibrium (existing flow $\boldsymbol{v}$), the situation is more serious because the linear relation is violated; Fick's law $\boldsymbol{f} = -D\nabla T$ may not be kept. Furthermore energy conservation is far complicated than equation (1.4),

$$\frac{\partial}{\partial t}(\rho e) + \nabla \cdot [\rho e \boldsymbol{v} + (P + \Pi) : \boldsymbol{v} + \boldsymbol{f}] = 0 \tag{1.10}$$

where $e = u + |\boldsymbol{v}|^2/2$ is the energy density, P and Π are the pressure tensor and stress tensor respectively. From Appendix A, entropy production rate with mass flow is represented as,

$$\dot{S} = \int \left[(\boldsymbol{f} + \Pi : \boldsymbol{v}) \cdot \nabla \left(\frac{1}{T} \right) + \Pi : \nabla \left(-f \boldsymbol{v} T \right) \right] d^3x \tag{1.11}$$

It is obvious that evaluating this functional is far more complicated than the linear case. Therefore we attempt to formulate the entropy production rate from the macroscopic side as consistent in thermodynamic laws.

1.3 H-mode

In fusion plasma, a state with improved energy confinement occurs because of an emergence of the transport barrier firstly observed by Wagner *et al.*[16]. The transition from the low-confinement phase (L-mode) to the high-confinement phase (H-mode) shows sudden and sharp increase of temperature and density gradient (Fig. (1.2)), by a factor of 2 and the width of the barrier is order of a few centimeters. The transition is observed when the entering heat flux exceeds threshold value. This threshold value intricately depends on various plasma parameters or experimental conditions. Many research has been done to understand L-H transition because more efficient plasma operation is attained by the improving of confinement. In experimental devices other than tokamak such as stellarator , H-mode is also observed [18].

Another characteristic feature is hysteresis [19]; The input power of H-L transition (backward transition) is lower than that of L-H transition (forward transition). In other words, once high confinement realized, the plasma sustain the improved state.

A number of proposal have been done to explain the mechanism of L-H transition. Recently suppression of turbulence is generally accepted as a cause

of transport barrier. Sheared $\boldsymbol{E} \times \boldsymbol{B}$ flow due to radial electric field provides a universal mechanism for the turbulence reduction[20, 21].

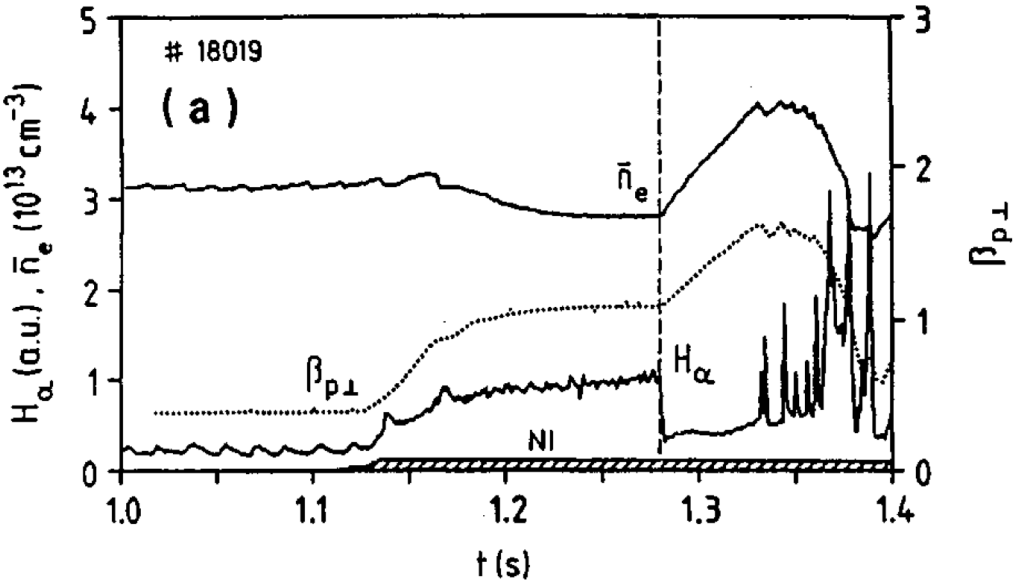

Figure 1.2: Evolution of plasma density $\bar{n_e}$, energy $\beta_{p\perp}$ and hydrogen Lyman alpha radiation H_α [17].

1.4 Objective

As we mentioned firstly, understanding self-organization phenomena in various turbulent systems is significantly fruitful. However usages of inherent mechanisms for each phenomena are unavoidable. Therefore we are motivated to describe these phenomena by deep and abstract mutual theory; The common term of any physical system is energy. In this research, we intend to reveal mathematical structure of the phenomenological model proposed by Yoshida & Mahajan which fulfills the above requirement.

In the next chapter, we prepare for analysis. In Sec. 2.1, we shall start by formulating a thermodynamic (phenomenological) model of turbulent heat transport in a tokamak boundary layer — an annular thin layer surrounding the high-temperature core plasma and connecting to cold (room temperature) heat bath. This thin layer set the stage for the plasma to self-organize a structure (ordered shear flow) which reduces the heat transport (or improve the plasma confinement and produces the so-called H-mode). The aim of this paper is not to analyze the "mechanism" of the self-organization, but is to elucidate the underlying mathematical structure that determines the bifurcation and stability. In Sec. 3.1, thermodynamic stability is discussed in "flux-driven system"

and "force-driven system" respectively. The state is proved to bifurcate to nonlinear in both case. In Sec. 3.2, we shall introduce thermodynamic functions by which we can represent the bifurcation of different states and measure the entropy production rate. The mini-max duality of entropy production rate will be explained by a Legendre transformation between the force-driven and flux-driven parameterizations of the thermodynamic function. In Sec. 3.3, we discuss how the hysteresis occurs. The application of this model is discussed in Chapter 3. We take one neoclassical model as a concrete example of H-mode and prove it equals our phenomenological model in a thin layer.

Chapter 2

Formulation of a thermodynamic model of plasma heat transport

2.1 Boundary Layer Model

Firstly, we follow the phenomenological model invented by Yoshida & Mahajan. The phenomenon they considered are highly developed turbulent system. While there exist various kinds of such a turbulent systems, for example

planet's atmosphere, H-mode is brought as a typical example; A sudden sharpening of the temperature gradient and a confinement efficiency improvement occur (bifurcation) at tokamak boundary layer when the entering heat flux exceeds some critical value. Developed disordered turbulence already exists at this boundary (Fig. 2.1 (c)), but an increase of heat creates order in turbulence and then raises temperature gradient (Fig. 2.1 (d)).

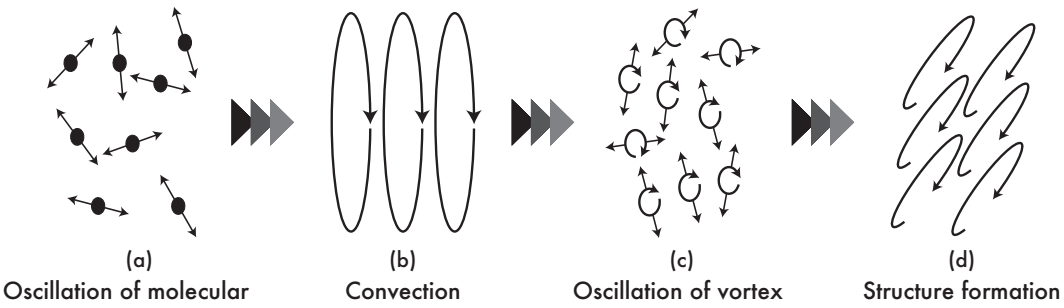

Figure 2.1: Bifurcation of fluid system. We intend to discuss the transition from (c) to (d).

H-mode has nonlinear heat transport through convection, while that in disordered turbulence is via linear dissipative L-mode. This is similar to a bifurcation from the linear dissipation state to the nonlinear convective state like Bénard Convection. The mechanism of this process has been proposed by many researchers; Suppression of turbulence by sheared flow originated from

$\boldsymbol{E} \times \boldsymbol{B}$ drift is one possibility of a explanation of the transport barrier[22]. Yoshida & Mahajan, on the other hand, illustrated bifurcation phenomena only with simple thermodynamics without considering electromagnetism and fluid mechanics. Here we note our intention is not to reveal the mechanism of H-mode but to find the backbone of structure formation that is common for various turbulent systems. In other words, we develop the theory that can be applied to any open system (independent to a mechanism).

The thermodynamics of idealized thin plasma layer, bounded from the internal core plasma and from the outside cold heat bath, is discussed. The inner-boundary temperature is T_1 and the outer-boundary is fixed at T_0 (heat bath). Heat flux flowing through this layer is represented as F. The plasma considered here is steady and relaxed enough; Flux F equals both to the energy injection rate and the energy dissipation rate. There is no mass flow across the layer. We set η as an impedance (inverse heat diffusivity) against F. Generally impedance η shows complicated response to controlling parameters. We, however, define η as sum of a linear term η_0 and a nonlinear term $\eta(P)$, because our interest is the bifurcation from linear state to nonliner state. P, determined later, is the power to drive the flow. Therefore the relation between F and T is written as,

$$T = T_0 + (\eta_0 + \eta(P))F \tag{2.1}$$

We define T_D as the temperature in diffusive process as P is absent ($T_D = T_0 + \eta_0 F$ keeping Fourier's law). In this ambient state, flux is represented by Fick's law $F = D\Delta T/\Delta x$ (constant through x direction), Δx is the thickness of the layer and D is the heat diffusion coefficient. This equals the steady condition $\nabla \cdot \boldsymbol{f} = 0$, whereas $\boldsymbol{f} = -D\nabla T$ is heat flow vector. Though coefficient D, however, cannot be constant in a state with flow, we will exhibit steady state condition derives $F = D\Delta T/\Delta x = \text{const}$ in chapter 4.

Our interest is not in this trivial flowless state but in extra power state. Figure 2.2 is the equivalent circuit of equation (2.1). The characteristic difference between this circuit and ordinary electric circuit is that flux (equivalent to current) is controlled.

To evaluate P as the available power to generate a flow, we subtract the work wasted in diffusive process, $F(1 - T_0/T_D)$, from the ideal Carnot-cycle work, $F(1 - T_0/T)$.

$$P = F\left(1 - \frac{T_0}{T}\right) - F\left(1 - \frac{T_0}{T_D}\right) = F\left(\frac{T_0}{T_D} - \frac{T_0}{T}\right) \tag{2.2}$$

We introduce efficiency factor a that measure the influence of the flow, then

multiply a to P as $\eta(P) \equiv aP$. The coefficient a is assume to be constant here, non-constant a will be discussed later.

Therefore equation (2.1) is rewritten as,

$$\Delta T^* = \frac{aF^2 T_0 \Delta T^*}{(T_D + \Delta T^*) T_D} \equiv g(\Delta T^*) \tag{2.3}$$

where $\Delta T^* \equiv T - T_D$ is the temperature increase by the occurrence of flow from linear state. This equation has two solutions,

$$T = \begin{cases} T_D \equiv T_1 \\ \dfrac{aF^2 T_0}{T_D} \equiv T_2 \end{cases} \tag{2.4}$$

Under the bifurcation condition, to be shown soon, T_2 overtakes T_1 in $F > F_\mathrm{c}$ whereas F_c is,

$$F_\mathrm{c} \equiv \frac{T_0}{\sqrt{T_0 a} - \eta_0} \tag{2.5}$$

This means the solution bifurcates when the heat flux F exceeds the critical value F_c. The first is a trivial solution when flow is absent. It is the second solution we seeking out; Higher temperature inhomogeneity is obtained. Figure 2.3 gives us graphical understanding. Two curves $y = \Delta T^*$ and $y = g(\Delta T^*)$

have the trivial intersection around the origin for any F. The second solution appears when F exceeds the critical value that is given by,

$$g'(0) = \frac{aF^2T0}{T_D^2} > 1 \tag{2.6}$$

Therefore the bifurcation condition is,

$$T_0 > \frac{\eta_0^2}{a} \tag{2.7}$$

We note if the edge temperature is too much low, bifurcation does not happen. The relation between F and T is plotted on Fig. 2.4. Under the bifurcation condition, two curves have intersection. As we discuss in Sec. 3.1, blue line is realized before the bifurcation and red line is realized after the bifurcation. The auxiliary lines indicate the mini-max of two solutions reverses which parameter, F or T, is chosen.

The important result is that impedance η increases when $F > F_c$. Increase of impedance causes rise of temperature gradient because the heat flux is given as an independent variable. Therefore, the entropy production rate is higher after bifurcation. This process can be easily understood by replacing (F, T, η) for the circuit variables (I, V, Z) as mentioned in Chapter 1.

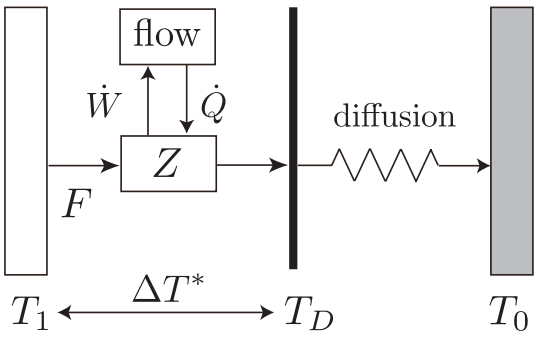

Figure 2.2: Equivalent circuit of the heat engine model [13]. Positive ΔT^* cause the mechanical energy of flow $\dot{W}$, equals $\dot{Q}$. This flow sustains temperature contrast (positive feed-back).

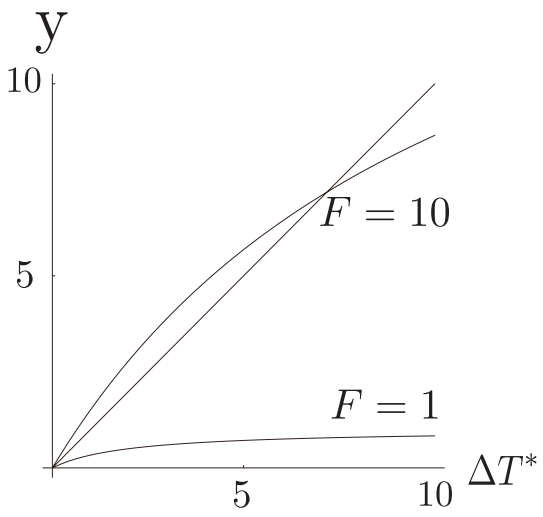

Figure 2.3: Graphical understanding of equation (2.3) [13]. Two curves intersect around origin for any F (trivial solution). Another solution appears when F exceeds critical value satisfying $g'(0) > 0$. Other parameters are $(T_0, a, \eta_0) = (1, 2, 1)$.

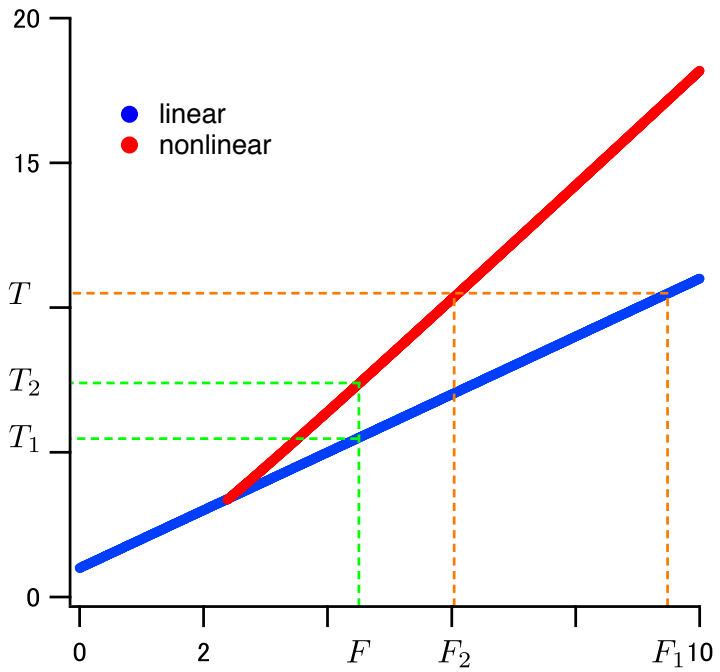

Figure 2.4: Plot of the relation between F and T (2.4). Dual mini-max of linear solution and nonlinear solution is exhibited; If F is constant, nonlinear solution is larger. Oppositely, if T is constant, nonlinear solution is smaller.

Since the nonlinear solution of equation (2.4) explicitly contains the variable a, assumption of non-constant a is believed to cause weird behavior after the bifurcation while the bifurcation itself is irrelevant to the shape of a. In section 3.3, we extend a as non-constant $a(T)$, and prove $a(T)$ with a certain shape causes hysteresis that has been actually observed in fusion experiments.

2.2 Thermodynamic function

A thermodynamic function (potential function) is introduced to overlook this model. In nature, various phenomena appear on critical points of some functional; In mechanics, a motion of a particle is along minimum of potential energy; Or in constant temperature equilibrium, minimum free energy state appears. Analogously we set the potential function of this model that gives the operation point as its variation. We write equation (2.1), even if $a = a(T)$ is a function of T, explicitly as $F = g(T)$ and integrate it by $1/T$. Following thermodynamic function is obtained.

$$-\Phi(\beta, F) = \int_{\beta_0}^{\beta_1} -g(T)d\beta + F\int_{\beta_0}^{\beta_1} d\beta, \quad (\beta \equiv 1/T) \tag{2.8}$$

$\Phi(\beta, F)$ is defined positive because the domain of integration is β_0 to β

(higher temperature to lower temperature).

As we will mention in Sec. 3.2, the first term of the right hand side of the equation (2.8) equals the variation of entropy production rate when the boundary temperature changes from T_0 to T. Therefore, the operation point of this model is not a critical point of the entropy production rate but of $\Phi(\beta, F)$. In other words, the second term plays important roll when flux F exists. The duality (minimum or maximum) is revealed by this function. The mechanism and condition of hysteresis is also explained qualitatively and quantitatively.

Chapter 3

Analysis of entropy production rate – stability, bifurcation and hysteresis

3.1 Stability of the model

Thermodynamic stability of this model must be investigated. Because more stable solution of equation (2.1) is realized. In this chapter, the each solutions of equation (2.1) with constant a is examined with F and T as independent variable respectively. The case a is not constant is discussed in Chapter 3.3.

3.1.1 Flux-driven system

Firstly, we consider the following chain of values when F is given. Fixing F as some value and having temperature perturbation δT,

$$\delta T \rightarrow \delta P = \frac{\partial P}{\partial T}\delta T = F\frac{T_0}{T^2}\delta T$$

$$\rightarrow \delta\eta = \frac{\partial \eta}{\partial T}\delta T = aF\frac{T_0}{T^2}\delta T$$

$$\rightarrow \delta T' = F\frac{\partial \eta}{\partial T}\delta T = aF^2\frac{T_0}{T^2}\delta T \equiv \alpha^F \delta T$$

When $\alpha > 1$, system is unstable because the temperature difference increases exponentially. The evolution of perturbation is $\delta T(t) = e^{\gamma t}\delta T(0)$ with $\gamma = (\ln \alpha)/\tau$ where τ is time constant.

Under the bifurcation condition (2.7), the stability of the linear solution in pre-bifurcation $F < F_{\rm c}$ ($T_1 > T_2$) state is,

$$\alpha_1^F = \frac{aT_0F^2}{T_1^2} = \frac{T_D}{T_1^2}\frac{aT_0F^2}{T_D} = \frac{T_2}{T_1} < 1 \tag{3.1}$$

The stability of the nonlinear solution in pre-bifurcation state is,

$$\alpha_2^F = \frac{aT_0F^2}{T_2^2} = \frac{T_D}{T_2^2}\frac{aT_0F^2}{T_D} = \frac{T_1}{T_2} > 1 \tag{3.2}$$

Therefore the linear solution appears before bifurcation. The stability of the linear solution in post-bifurcation $F > F_{\mathrm{c}}$ ($T_1 < T_2$) is,

$$\alpha_1^F = \frac{aT_0F^2}{T_1^2} = \frac{T_D}{T_1^2}\frac{aT_0F^2}{T_D} = \frac{T_2}{T_1} > 1 \tag{3.3}$$

The stability of the nonlinear solution in post-bifurcation is,

$$\alpha_2^F = \frac{aT_0F^2}{T_2^2} = \frac{T_D}{T_2^2}\frac{aT_0F^2}{T_D} = \frac{T_1}{T_2} < 1 \tag{3.4}$$

Therefore, after the bifurcation point, the linear solution is unstable and the nonlinear one is stable, then nonlinear state is realized. Evolution of α is plotted on Fig. 3.1. This can be interpreted that constant flux and larger impedance give more available power to drive the flow (ZI^2).

3.1.2 Temperature-driven system

Next we contrarily discuss the system which the temperature is controlled. When T is given, the equation of this model is rewritten as,

$$F = C(T - T_0) \tag{3.5}$$

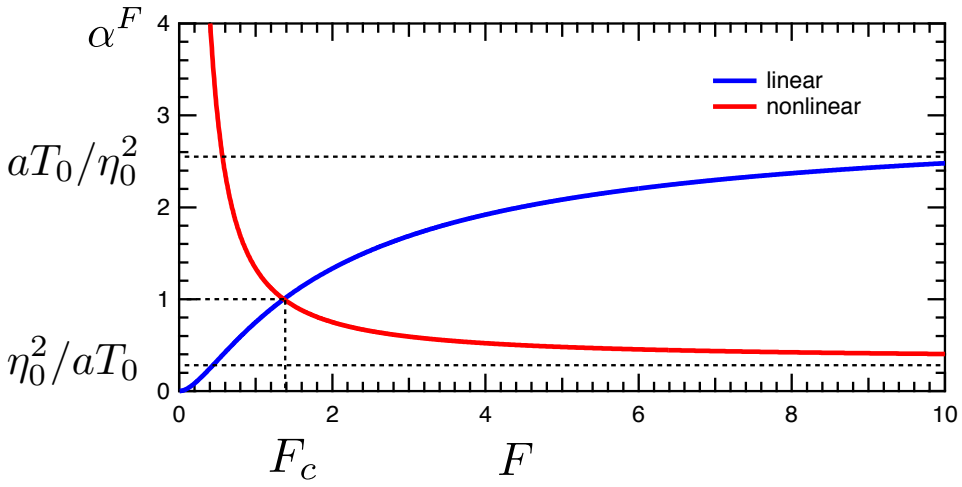

Figure 3.1: Evolution of growth rate of the linear and the nonlinear solution as a function of flux

Here we define heat diffusion coefficient C (conductance) as

$$C \equiv \frac{1}{\eta} = \frac{1}{(\eta_0 + aP)} \tag{3.6}$$

This is solved explicitly as a function of T,

$$F = \frac{\eta_0 T + \sqrt{(\eta_0 T)^2 + 4aT_0^2 T}}{2aT_0} \equiv -g(T) \tag{3.7}$$

Bifurcation occurs at the critical temperature,

$$T_{\rm c} = \frac{T_0\sqrt{aT_0}}{\sqrt{aT_0} - \eta_0} \tag{3.8}$$

We can imagine the chain event in the same way as Sec. 3.1.1. The perturbation of flux δF becomes,

$$\delta F \rightarrow \delta C = \frac{\partial C}{\partial F}\delta T$$

$$\rightarrow \delta F' = (T - T_0)\frac{\partial C}{\partial F}\delta F \equiv \alpha^T \delta F$$

$$\begin{aligned} \alpha^T &= -\frac{(T - T_0)}{(\eta_0 + aP)^2}\frac{\partial}{\partial F}(aP) \\ &= -\frac{(T - T_0)}{\left[\eta_0 + aT_0F\left(\frac{1}{T_D} - \frac{1}{T}\right)^2\right]^2}\left[aT_0\left(\frac{1}{T_D} - \frac{1}{T}\right) - aT_0F\frac{\eta_0}{T_D^2}\right] \end{aligned} \tag{3.9}$$

The stability of the linear solution is calculated by substituting $F = F_1$,

$$\alpha_1^T = \frac{aT_0}{\eta_0^2}\left(1 - \frac{T_0}{T}\right)^2 \tag{3.10}$$

This is monotonically increasing in $T > T_0$ and equals to 1 at the bifurcation point $T = T_c$. And $\lim_{F\to\infty}\alpha_1^T = \eta_0^2/aT_0$. The linear solution becomes therefore stable in pre-bifurcation and unstable in post-bifurcation.

We now discuss the nonlinear solution case. Substituting $F = F_2$,

$$\alpha_2^T = \frac{2T}{a(T-T_0)T_0(\eta_0 + \sqrt{(\eta_0^2 T + 4aT_0^2)T})} \times$$

$$[\eta_0^4 T^2 + 4a\eta_0^2 T_0^2 T + 2a^2 T_0^3 (T_0 - T) + \tag{3.11}$$

$$(\eta_0^3 T + 2a\eta_0 T_0^2)\sqrt{(\eta_0^2 T + 4aT_0^2)T}\Big]$$

This is monotonically decreasing function in $T > T_0$ and becomes 1 at the bifurcation point. And $\lim_{F\to\infty} \alpha_2^T = aT_0/\eta_0^2$.

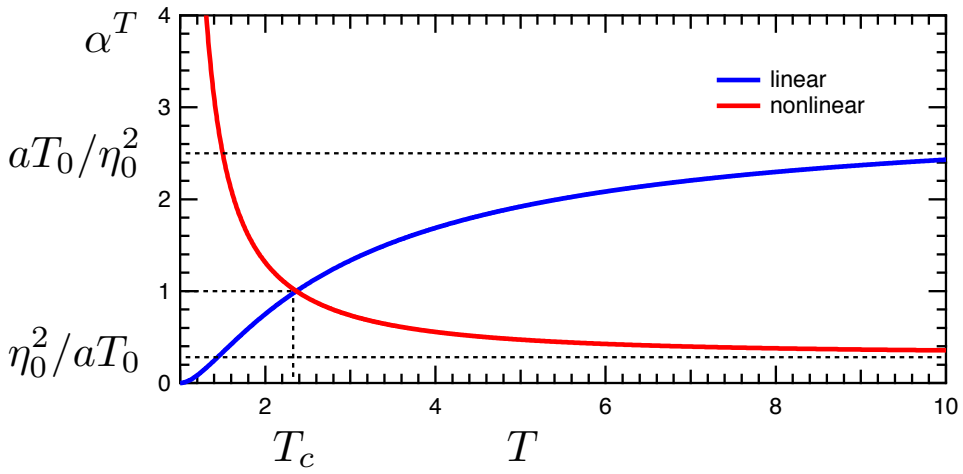

Figure 3.2: Evolution of growth rate of the linear and the nonlinear solution as a function of temperature

Figure.3.2 is obtained and this means the system bifurcates to a nonlinear

solution same as for the flux-given system. This is contrary to the interpretation in the end of last subsection; The available power to drive the flow seems to be smaller this time (V^2/Z). In summary, the system bifurcates to nonlinear solution regardless of our selection of independent variable.

3.2 Legendre transformation about entropy production rate

As we mentioned in Sec. 1.2 entropy production rate is written as a volume integral of the inner product of irreversible flow and thermodynamic power (equation 1.1). We emphasize again that minimization of entropy production rate does not derive Fourier's law and that even formulating entropy production rate is difficult in a state far from equilibrium. We therefore define $\boldsymbol{f}$ from the phenomenological model as consistent in thermodynamics.[13]

Firstly we review the discussion of thermodynamic relation of general heat engine [13]. First law of thermodynamics is,

$$dU = \delta Q - \delta W \tag{3.12}$$

where U is the internal energy, Q is heat the system obtains and W is work the system does outwards. The sign d denotes exact differentiation and δ denotes non-exact differentiation. In non-equilibrium state, we can distinguish reversible processes and irreversible processes with second law of thermodynamics as,

$$\delta Q = T(dS - \delta S_i) \tag{3.13}$$

where S_i is internal entropy production by irreversible process. Equation (3.12) is rewritten as,

$$\begin{aligned} \delta W &= \delta Q - T_0 dS - (dU - T_0 dS) \\ &= \left(1 - \frac{T_0}{T}\right) \delta Q - T_0 \delta S_i - (dU - T_0 dS) \end{aligned} \tag{3.14}$$

Time derivative of this equation is obtained.

$$\dot{W} = \left(1 - \frac{T_0}{T}\right) \dot{Q} - T_0 \dot{S}_i - \frac{d}{dt}(U - T_0 dS) \tag{3.15}$$

To obtain global thermodynamic relation of a steady system, equation (3.15) is integrated over total domain, noting integral of the third term of right hand side (consisted only of state variable U and S) equals zero.

$$\int \dot{W} dM = \int \left(1 - \frac{T_0}{T}\right) \dot{Q} dM - T_0 \int \dot{S}_i dM \tag{3.16}$$

where $dM \equiv \rho d^3x$. Now we apply this general steady heat engine relation to the model (2.1).

A heat flow vector $\boldsymbol{f}$ ($\dot{Q}\rho = -\nabla \cdot \boldsymbol{f}$) is introduced. The first term of right hand side of equation (3.16) is manipulated, divided by T_0,

$$\begin{aligned} -\int \left(\frac{1}{T_0} - \frac{1}{T}\right) \nabla \cdot \boldsymbol{f} d^3x &= -\int \nabla \cdot \left[\left(\frac{1}{T_0} - \frac{1}{T}\right) \boldsymbol{f}\right] d^3x \\ &\quad - \int \boldsymbol{f} \cdot \nabla \left(\frac{1}{T}\right) d^3x \qquad (3.17) \\ &= \left(\frac{1}{T_0} - \frac{1}{T}\right) F - \int \boldsymbol{f} \cdot \nabla \left(\frac{1}{T}\right) d^3x \end{aligned}$$

Substituting this into equation (3.16),

$$\int \dot{W} dM = \left(1 - \frac{T_0}{T}\right) F - T_0 \int \boldsymbol{f} \cdot \nabla \left(\frac{1}{T}\right) d^3x - T_0 \int \dot{S}_i dM \tag{3.18}$$

This approves in a general long-term averaged heat engine. The left hand side ($\int \dot{W} dM$) equals zero in a steady state, because global mechanical energy

is saturated. Finally we obtain entropy production rate from thermodynamic law.

$$\int \dot{S} dM \equiv \int \boldsymbol{f} \cdot \nabla \left(\frac{1}{T} \right) d^3x - T_0 \int \dot{S}_i dM = \left(\frac{1}{T_0} - \frac{1}{T} \right) F \tag{3.19}$$

Now we can deduct the meaning of S_i as the entropy production with structure formation; In diffusive process $\nabla \cdot \boldsymbol{f} = 0$ holds, then S_i equals zero. S_i denotes the increase from the diffusive entropy production. The entropy production rate is determined only by boundary values (T, T_0, F) fortunately. This is a strong affirmation because entropy production rate in general steady state (even with flow) is represented as a simple boundary term, while describing entropy production from fluid mechanical side (equation (A.10)) is quite complicated. Now we know, from the discussion of chapter 3.1, that the solution bifurcates to nonlinearity regardless of the independent variable we select. Figure 2.4 obviously tells us constant F yields nonlinear solution as larger temperature gradient. On the other hand, nonlinear solution given by constant T is smaller flux. So we can conclude, from equation(3.19), that the former means larger entropy production rate and the latter means smaller entropy production rate (Fig.3.3).

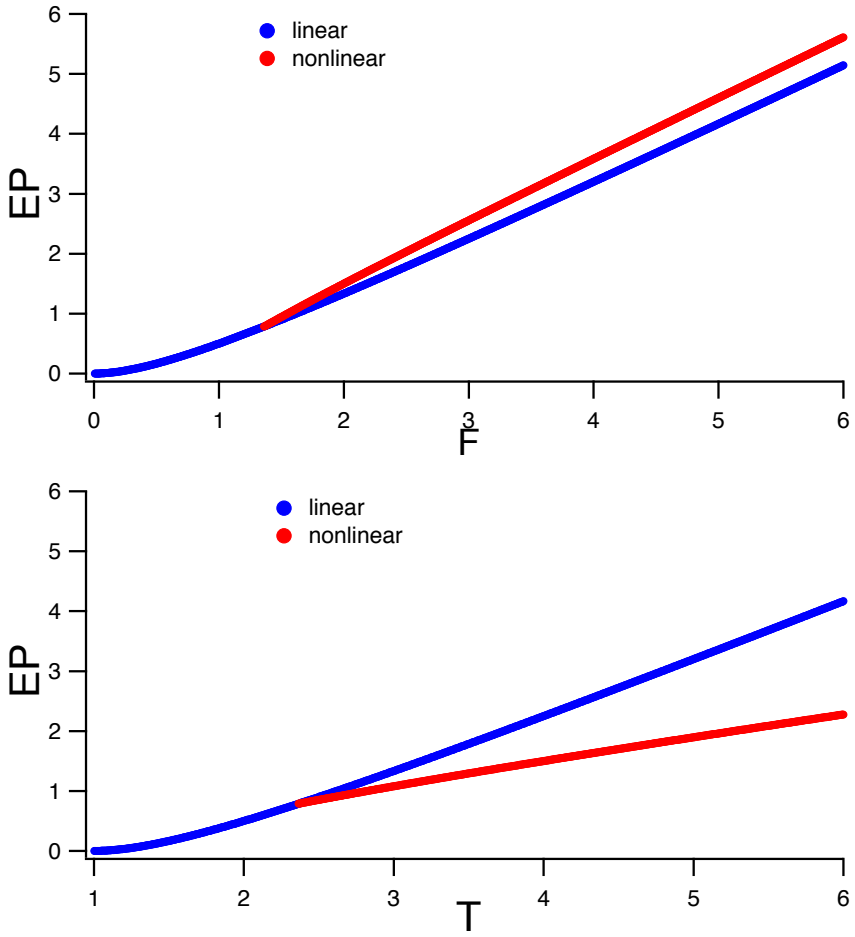

Figure 3.3: Evolution of EP.

Top: Controlling variable is flux. EP of nonlinear solution is larger.

Bottom: Controlling variable is temperature. EP of nonlinear solution is smaller.

What does it mean that the exchange of independent variables causes the reversal of "maximum" and "minimum"? Entropy production rate (1.1) in one dimension is written as,

$$\dot{S} = \int_{x_0}^{x_1} -g(T)\frac{d}{dx}\left(\frac{1}{T}\right) dx \tag{3.20}$$

An attention is required that this $\dot{S}$ differs from equation (3.19). This equals to the first term of the right hand side of the equation (2.8). Therefore, the operation point of this model is not a critical point of the entropy production rate but of $Q(\beta, F)$. This is why the minimization of equation (1.2) cannot derive phenomenological relation (2.1).

On the operation point, the following equation holds,

$$\frac{\partial \Phi(\beta, F)}{\partial \beta} = \frac{\partial \dot{S}(\beta)}{\partial \beta} + F = 0 \tag{3.21}$$

$\Phi(\beta, F)$ becomes Legendre transformation about $\dot{S}(\beta)$ under the above condition. $\Phi(\beta, F)$ is written as $\Phi(F)$ because

$$d\Phi = \frac{\partial \Phi}{\partial \beta} d\beta + \frac{\partial \Phi}{\partial F} dF = (\beta - \beta_0) dF. \tag{3.22}$$

That is to say, the "entropy production rate as a function of temperature" ($\dot{S}(\beta)$) is transformed into the "entropy production rate as a function of flux"

$(\Phi(F))$. The following dual relation is also obtained.

$$\frac{\partial \dot{S}}{\partial F} = -F, \quad \frac{\partial \Phi}{\partial F} = \beta - \beta_0 \tag{3.23}$$

$\dot{S}(\beta)$ is plotted in Fig.3.4. When we choose T as independent variable and change it as $T_0 \to \infty$, a change on Fig.3.4 is $\beta_0 \to 0$. It can be seen that the entropy production rate of the nonlinear solution is smaller. The F-controlled case is discussed next. Choosing F as an independent variable equals the problem to drawing a tangent line which has an inclination $-F$ in Fig.3.4 because Legendre transformation is a transformation that gives a tangent line (Appendix B). After the bifurcation $F > F_c$, the entropy production rate of the nonlinear solution is higher than that of the linear solution which has the same slope of the nonlinear solution.

This Legendre transformation is the mechanism of duality of the maximum and minimum caused by the exchange of independent variables on Fig.3.3. It is to be noted that the word "maximum" or "minimum" means not a global maximum or minimum but the alternative of large or small. A global minimum or maximum does not suitable for our heat engine as we mentioned before.

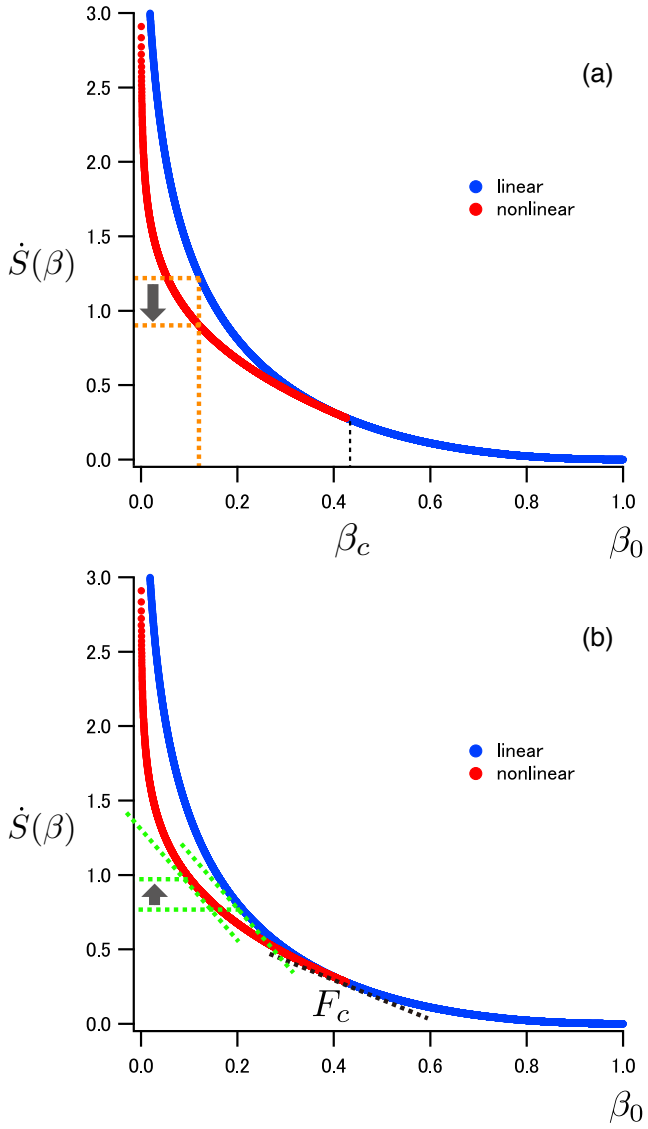

Figure 3.4: Plot of $S(\beta)$. (a) : β is controlled. After the bifurcation point β_c, entropy production of nonlinear solution is smaller.

(b) : F is controlled. A point having inclination of $-F_c$ is the bifurcation point. In this case, entropy production is larger.

3.3 Condition of hysteresis

It is widely known that H-mode shows hysteresis against the input of heat. Figure 2.4, however, does not bring out hysteresis, then the model used above is extended to be able to realize hysteresis. This extension also tells us a condition of hysteresis. To be concrete, though we have assumed the coefficient of impedance a as constant, some damping seems to take place at the high temperature state and the impedance may rise. Then we let the coefficient of impedance have a dependence of temperature as $a(T)$. Ψ is introduced to derive the condition of hysteresis as $\Psi(F,T) \equiv T - T_0 - \eta F$. Considering the T derivative of Ψ,

$$\frac{\partial \Psi}{\partial T} = 1 - \frac{a(T) T_0 F^2}{T^2} - FP(T)\frac{\partial a(T)}{\partial T} \tag{3.24}$$

Therefore, when the following condition,

$$\frac{\partial a(T)}{\partial T} > \frac{1}{FP(T)}\left(1 - \frac{T_1}{T_2}\right) \quad (>0) \tag{3.25}$$

holds, the implicit function theorem is violated and $\Psi(F,T)$ does not have a unique solution about F (it has multiple solutions). From the experimental point of view, measurable quantity is not $a(T)$ but η. Therefore the condition

of hysteresis expressed by η is more useful. Equation (3.25) is rewritten as,

$$\frac{\partial \eta}{\partial T} > \frac{1}{F} \tag{3.26}$$

If $a(T)$ increases sharply about T as in Fig. 3.5, or $\eta(T)$ increases sharply like in Fig. 3.6, there appears multiple solutions which is represented by a folding structure in Fig. 3.7. Graphical understanding of the bifurcation is shown in Fig. 3.8 that is the solution of equation (2.3).

Stability around multiple solutions is going to be discussed because the middle solution must be unstable for hysteresis to occur. Same as Sec. 3.1.1, we set F as an independent variable and calculate the growth rate α.

$$\alpha^F = F\frac{\partial \eta}{\partial T} = F\left(a(T)\frac{\partial P}{\partial T} + P\frac{\partial a(T)}{\partial T}\right) \tag{3.27}$$

The term about $\partial a(T)/\partial T$, that is vanished in the case $a(T)$ is constant, is added to α in Sec. 3.1.1. We can prove, by substituting (3.25) into (3.27), the solution satisfying the condition of folding (3.25) is always unstable ($\alpha > 1$).

Figure 3.9 is the plot of $\dot{S}(\beta)$ satisfying (3.25). When the nonlinear solution has a folding structure as in Fig. 3.7, $\dot{S}(\beta)$ has an inflection point. We can draw multiple tangent lines if F is selected as independent variable. This is the

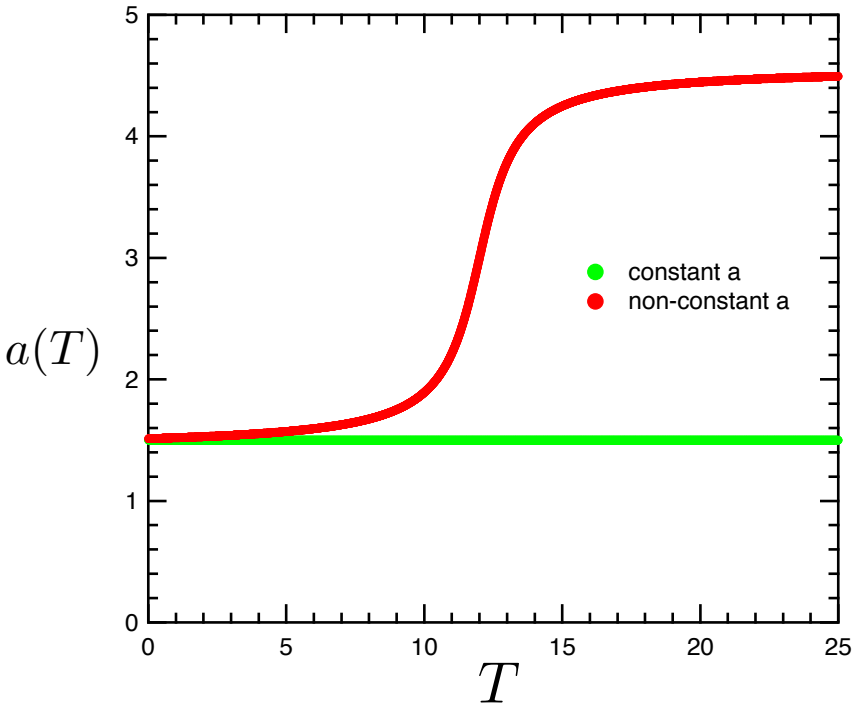

Figure 3.5: Shape of $a(T)$. Red: hysteresis occurs. Green: hysteresis does not occur.

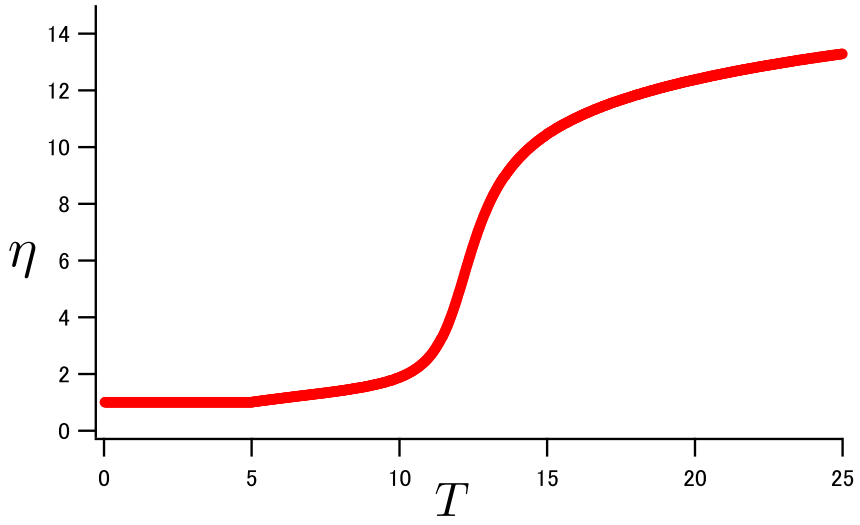

Figure 3.6: Shape of η with hysteresis.

reason why β jumps to a far value; If you go along β axis, there never occurs jump of solution as long as a is only the function only of T. Therefore the jump of solution is an unique feature of the tangent line problem. The conclusion is that when entropy production rate is warped to have an inflection point, selection of F as controlling parameter causes a jump in the solution and hysteresis.

Noteworthy feature is that this Legendre transformation is against non-convex function whereas ordinary Legendre transformation in both thermodynamics and analytical mechanics is assumed to be against convex function.

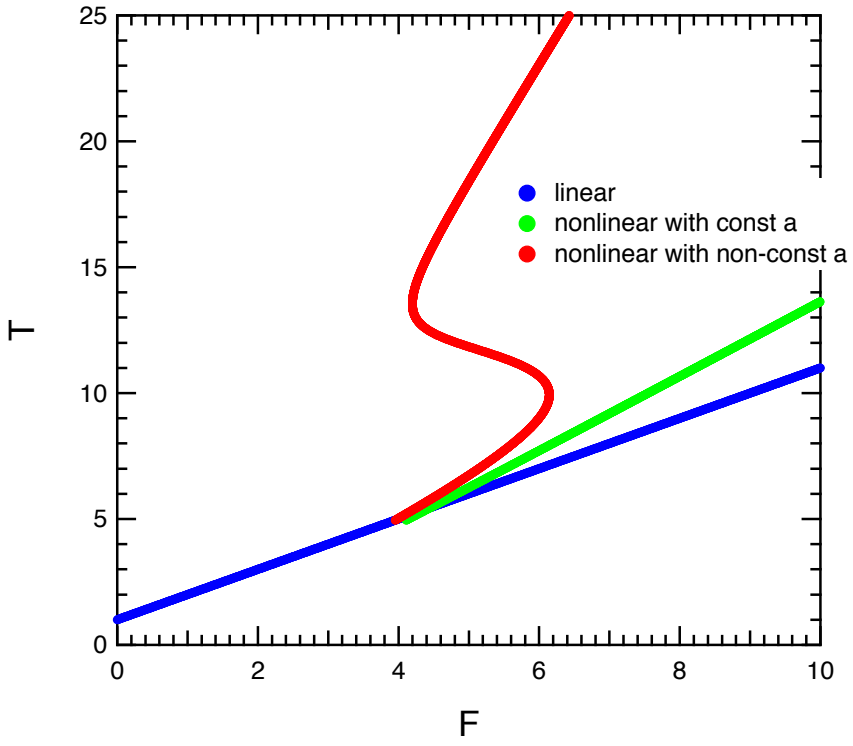

Figure 3.7: Relation between F and T. Blue: linear solution of (2.4). Red & Green: nonlinear solution; the colors correspond to Fig. 3.5

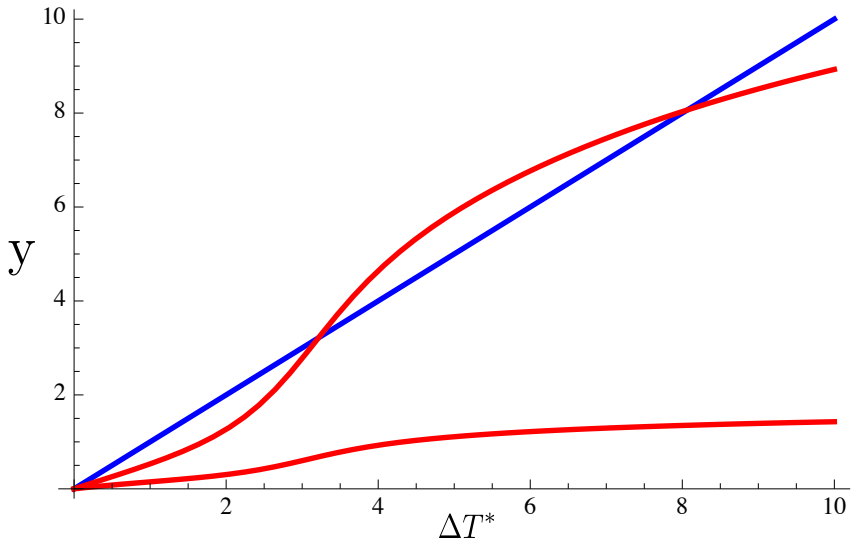

Figure 3.8: Graphical understanding of the bifurcation as in Fig. 2.3.The solution bifurcates to multiple solutions.

Here we find Legendre transformation against non-convex function derives hysteresis.

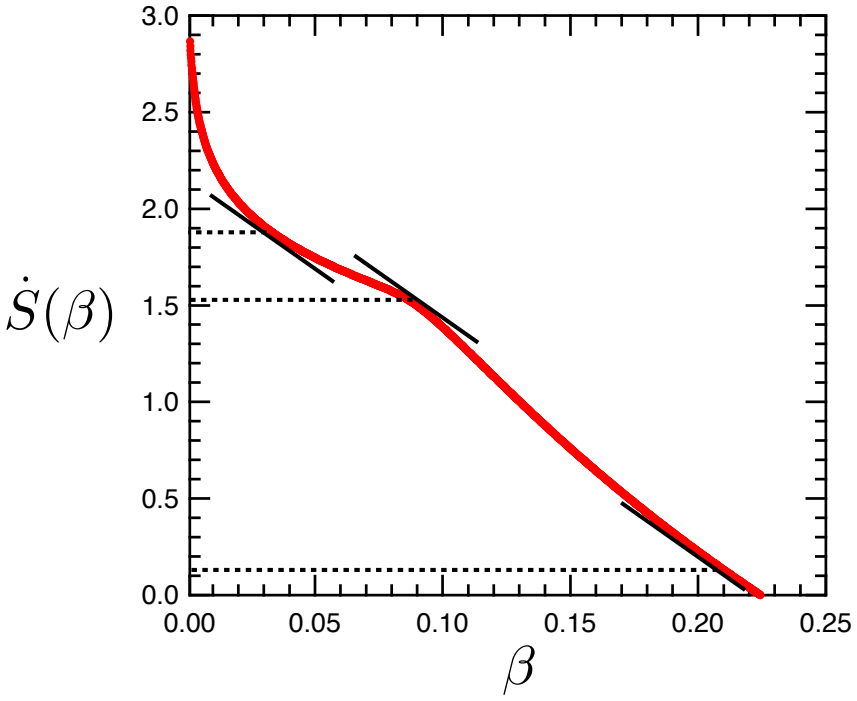

Figure 3.9: Profile of $\dot{S}(\beta)$ with hysteresis. Since the selection of F as independent variable means a tangent line problem, large nonlinearity, so as to $\dot{S}(\beta)$ having an inflection point, causes a jump to further β.

Finally we discuss about the term $\Phi(\beta, F)$ introduced in (2.8). As we mentioned in the last subsection, $\Phi(F)$ is Legendre "transformed" term. In

equilibrium thermodynamics, definition of Helmholtz free energy (B.2) is interpreted that internal energy U is put a restriction of TS. Analogously $\Phi(\beta)$ is obtained as a consequence of putting a restriction $F(\beta - \beta_0)$ on $\dot{S}$. The working point of this model is critical point of $\Phi(\beta, F)$.

$\Phi(\beta, F)$ with three representative F is plotted on Fig 3.10. $\Phi(\beta)$ has two stable maximum points and one unstable minimum point between these two around $F = 5$. Upon increasing F (forward process), the right maximum point is realized until it becomes an inflection point (around $F = 6$). When the right critical point becomes an inflection point, bifurcation towards the left maximum point occurs. Upon decreasing F (backward process), however, bifurcation does not occur until $F = 4$ because the unstable middle solution prevents the transition. Conceptual diagram is shown in Fig. 3.11; A stroke of F exhibits hysteresis.

Parameter dependence of $a(T)$ or η shall be speculated. The area of hysteresis loop plays an important roll because larger area means the system bifurcates to a further point. Here we simply set $a(T)$ as $B \arctan(T - A) + C$ that satisfies the condition of hysteresis (3.25). We independently changed parameters A, B and C in Fig. 3.12 (a), (b) and (c) respectively. In Fig. 3.12 (a), the temperature at the bifurcation point of impedance is varied while

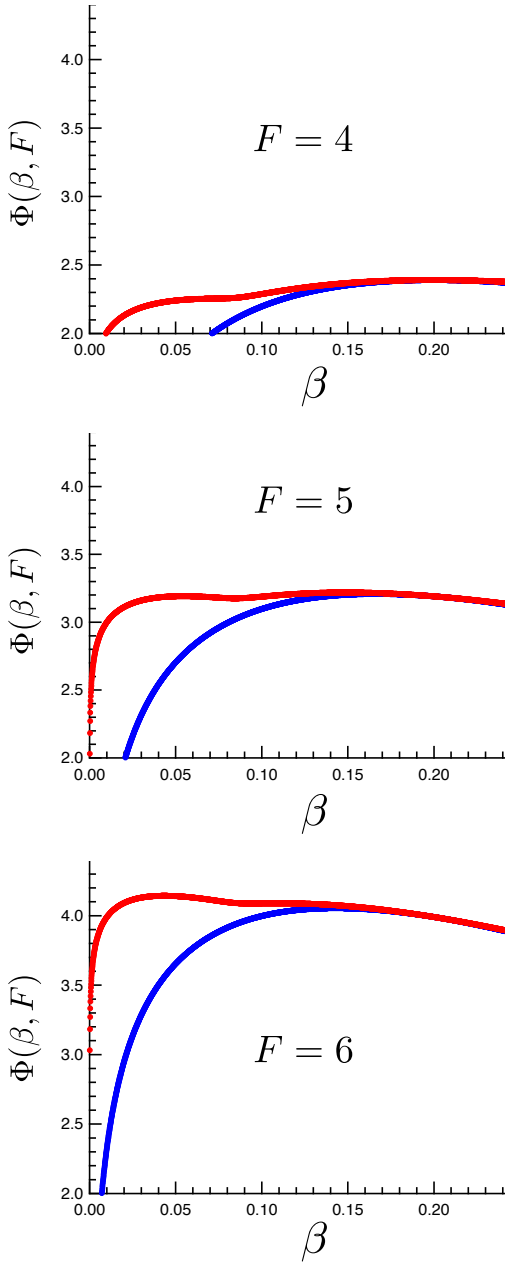

Figure 3.10: $\Phi(\beta, F)$ satisfying (3.25). Blue: linear solution of (2.4) –convex curve–. Red: nonlinear solution –non-convex curve–. From the top $F = 4, 5, 6$ respectively.

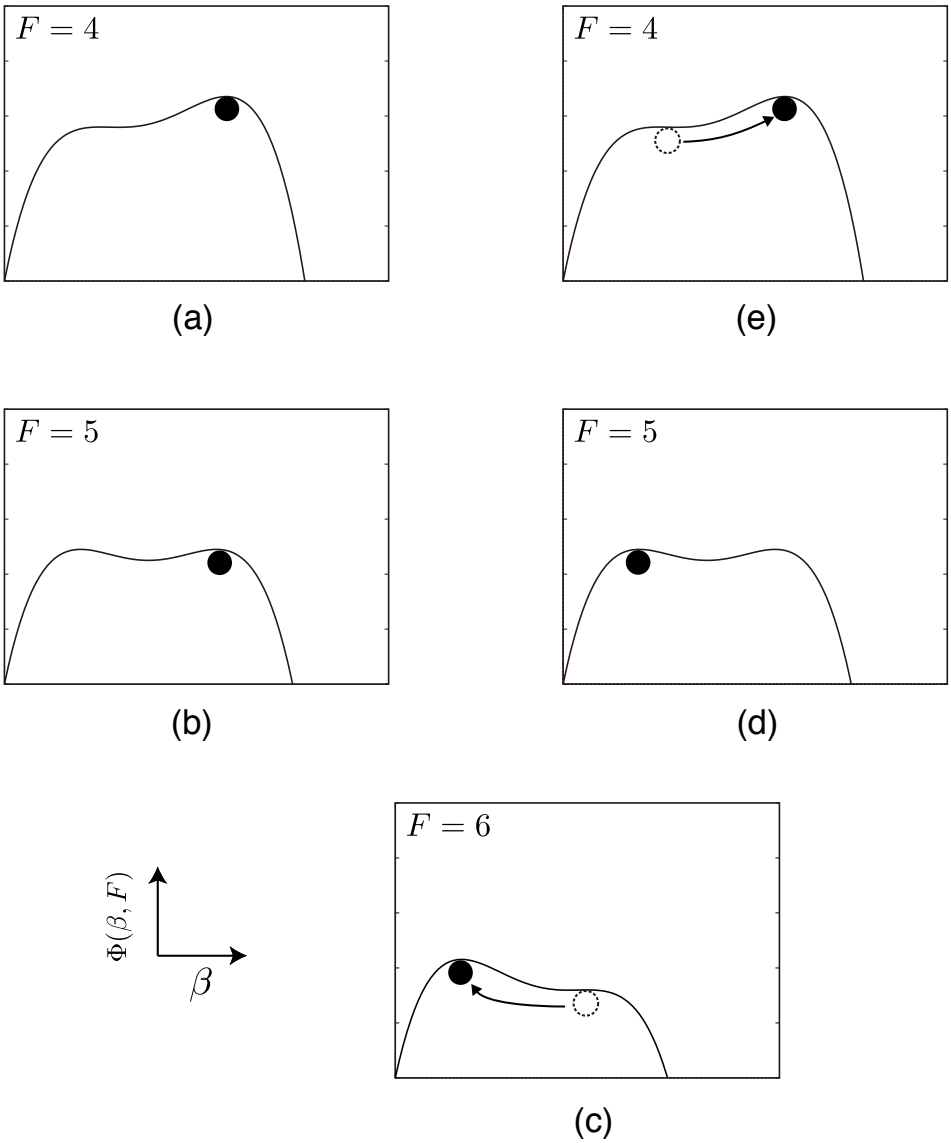

Figure 3.11: Conceptual diagram of Fig. 3.10. The global maximum of $\Phi(\beta, F)$ is the operation point. Transition occurs on (c) in forward process and on (e) in backward process.

the amplitude of impedance transition is kept constant. The area increases as the temperature of bifurcation points getting larger. In Fig. 3.12 (b), by contraries, the amplitude is varied with the critical temperature kept constant. In Fig. 3.12 (c), the gradient of impedance at the point of linear-nonlinear transition is changed. We can conclude , in any case, as the temperature of the first critical point in $F - T$ diagram (that is experimentally observed as the bifurcation point) becomes larger, the area of hysteresis loop also becomes larger. More precise quantitative discussion of parameter dependence will be discussed in Chapter 4.

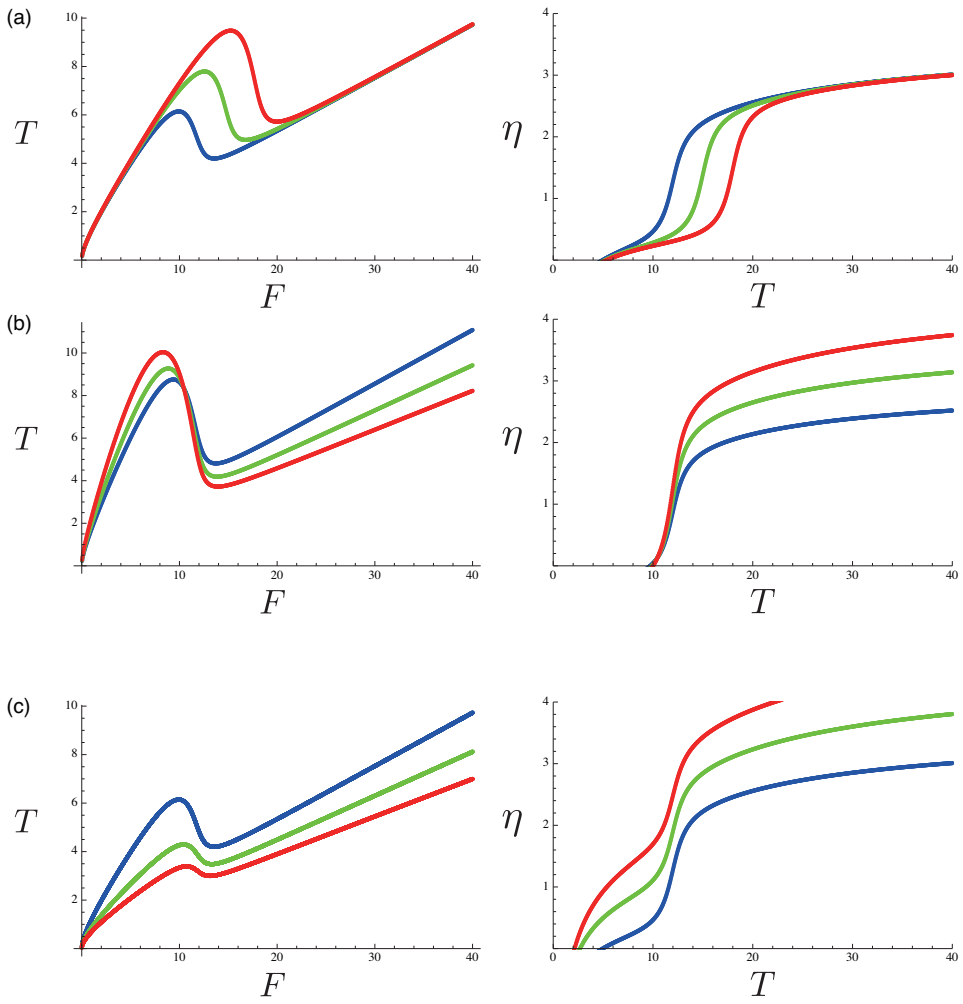

Figure 3.12: Qualitative dependence of impedance. Top: the temperature of bifurcation point. Middle: the amplitude of impedance bifurcation. Bottom: the gradient of impedance at the point of linear-nonlinear bifurcation.

Chapter 4

Discussions on the mechanics

We have constructed the phenomenological model and have analyzed it so far. This model is written only by an exchange of energy. There is, therefore, no doubt that this model is universally applied to various open systems. The story, that large flux creates order in a system and the order derives further temperature contrast, is independent to the mechanisms between flux and order. For example, the neoclassical theory of poloidal rotation induced by radial electric field is thought to be one possible mechanism of H-mode. A zonal flow induced by β effect in planet's atmosphere is also this kind of mechanism. Of course mechanism independent theory is the deepest and the most abstract theory, but there exists some distance from realistic phenomena. In this chapter, we

take an example of neoclassical model explaining H-mode [23] and prove it is one of the concretization of our model.

4.1 Neoclassical model of L-H transition

Hinton *et al.* proposed the scenario that can explain bifurcation and hysteresis of L-H transition by neoclassical plasma poloidal rotation[23, 24]. Here we review the equations of essential part to obtain the relation between heat flux and temperature gradient though our intention is not in its derivation. On a toroidal coordinate, poloidal ion velocity is thought to play an important roll to an improvement of confinement. Bigrali *et al.* proposed that turbulence can be greatly reduced by stable sheared poloidal flow[25]. Experiments also showed sudden and significant increase of poloidal rotation between L-H transition [26]. The suppression of turbulent flow around the plasma edge is therefore expected to be the cause of reduction of radial heat transport.

The poloidal rotation flow is shown to be determined only by the temperature gradient and to be proportional to the temperature gradient from standard neoclassical theory [27].

$$u_\theta = -\frac{c}{eB}\mu(\nu_{*i})\frac{\partial T}{\partial r} \tag{4.1}$$

the coefficient is evaluated as,

$$\mu(\nu_{*i}) \simeq 1.7 + \frac{\mu_1}{(\nu_{*i})^2}$$

where μ_1 is less than unity. This translation velocity u_θ to temperature gradient $\partial T/\partial r$ is the "mechanism" we mentioned above.

Using this estimation, radial gradient of u_θ is written as,

$$\frac{\partial u_\theta}{\partial r} = -\frac{4c\mu_1}{eB(\nu_{*i})^2 T}\left(\frac{\partial T}{\partial r}\right) \tag{4.2}$$

Next, thermal relation must be modeled. The local heat flux is modeled as the sum of neoclassical contributions and flowless diffusive heat flux divided by the effect of shear suppression of turbulence. Heat diffusion coefficient is represented as,

$$\kappa \equiv \kappa_n + \frac{\kappa_a}{1 + \gamma_a(\partial u_\theta/\partial r)^2} \tag{4.3}$$

Substituting equation (4.2),

$$\kappa = \kappa_n + \frac{\kappa_a}{1 + \lambda_a (\partial T/\partial r)^4} \tag{4.4}$$

with λ_a defined as,

$$\lambda_a \equiv \frac{\gamma_a}{(\nu_{*i})^4} \left(\frac{4c\mu_1}{eBT} \right)^2$$

Since the coefficients κ_n, κ_a and λ_a are numerical constant, we cannot specify these as measurable value. The local heat flux is written multiplying diffusion coefficient by negative temperature gradient.

$$Q(\frac{\partial T}{\partial r}) = -\kappa \frac{\partial T}{\partial r} \tag{4.5}$$

If we select the coefficients κ_n, κ_a and λ_a appropriately, the function Q has multiple critical points against $\partial T/\partial r$ (Fig. 4.1).

This figure obviously resembles Fig. 3.7. In the same manner of our model, heat flux is chosen to be independent variable and the solution bifurcate to larger temperature contrast state when flux Q exceeds critical Q_c.

The most characteristic difference to our model is the existence of information about radial profile. The radial temperature gradient is assumed to

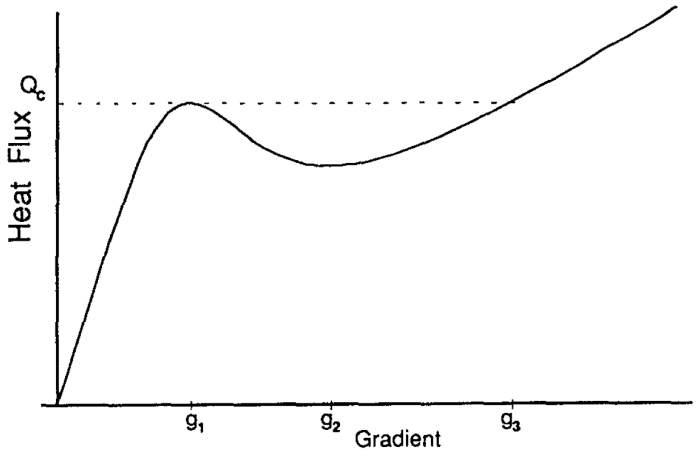

Figure 4.1: Relation between heat flux and temperature gradient at edge[23], with similar profile of Fig. 3.7.

be constant in our model as $\partial T/\partial r \simeq \Delta T/\Delta r$ because the region we are considering is very thin. We can obtain the equilibrium temperature profile by integrating following equation,

$$-\kappa \frac{dT}{dr} = Q(r) \tag{4.6}$$

where $Q(r)$ is the heat flux at radius and varies linearly via r direction. Then $Q(r)$ is estimated as, After all, temperature profile is obtained by solving the next ordinary differential equation.

$$-\left(\kappa_n + \frac{\kappa_a}{1+\lambda_a(dT/dr)^4}\right)\frac{dT}{dr} = Q(a)\frac{r}{a} \tag{4.7}$$

Now we show this neoclassical model converges to our model in the same thin layer where an approximation such as temperature gradient becomes constant.

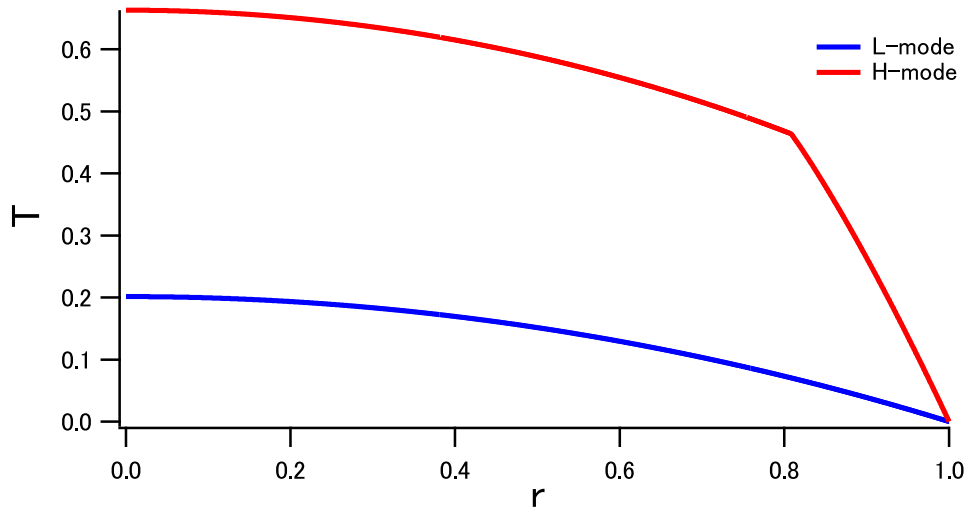

Figure 4.2: Radial profile of temperature. The steep temperature gradient is exuded.

4.2 Thin layer approximation of the neoclassical model

We focus on the domain in which heat flux shall be constant. The left hand side of equation (4.7) becomes $Q(a)$. Solving this ordinary differential equation, Fig. 4.3 is obtained.

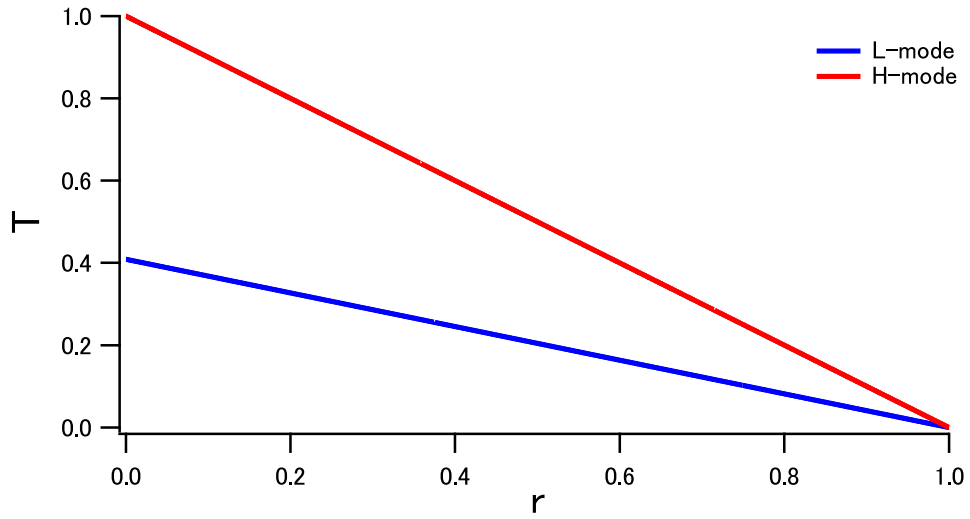

Figure 4.3: Radial temperature profile under the thin layer approximation. The temperature gradient is assumed to be constant.

The constant radial gradient of temperature is easily figured out. Figure 4.4 is magnified view of Fig. 4.2 around $0.8 < r < 1.0$ (edge). The similarity

of these two figures indicates that we can deem the temperature gradient to be constant ($\partial T/\partial r \simeq \Delta T/\Delta T$) and heat flux to be constant ($\partial Q(r)/\partial r \simeq 0$) in the thin layer.

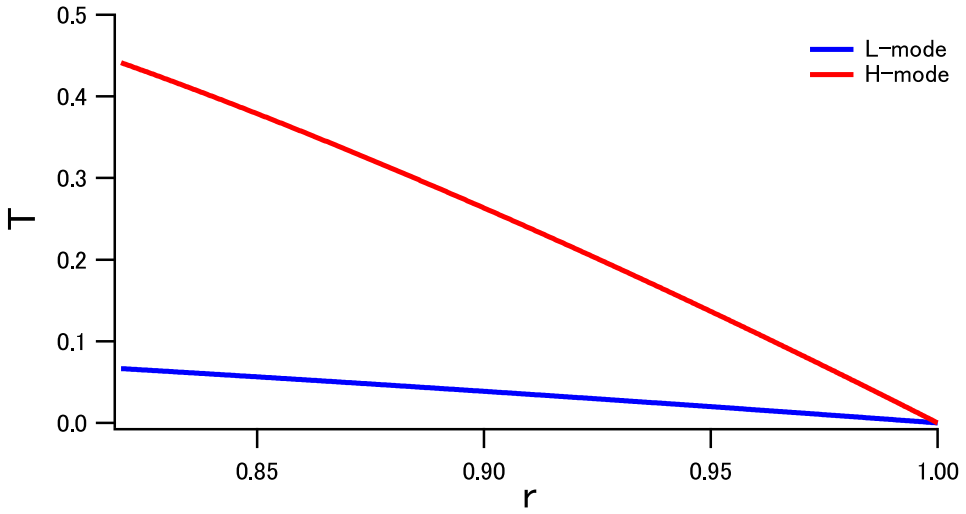

Figure 4.4: Radial temperature profile around $0.8 < r < 1.0$. Linear profile is obtained again in this edge thin layer.

Therefore equation (4.7) is written as,

$$-\left(\kappa_n + \frac{\kappa_a}{1+\lambda_a(T-T_0)^4/(\Delta r)^4}\right)\left(-\frac{T-T_0}{\Delta r}\right) = F \tag{4.8}$$

This is compatible to equation (2.1) of our model. The discussions of chapter 3 can be applied to this form of equation. The condition of hysteresis (3.26) becomes,

$$\frac{\partial F}{\partial T} = \frac{T - T_0}{\Delta r}\frac{d\kappa}{dT} + \frac{\kappa}{\Delta r} < 0 \tag{4.9}$$

Therefore the condition is that there exists positive α such that

$$\frac{\kappa_n \alpha^2 + (2\kappa_n - 3\kappa_a)\alpha + \kappa_n + \kappa_a}{(1+\alpha)^2} < 0$$

is satisfied. The inequality is solved as $\kappa_a/\kappa_n > 16/9$.

Though this final inequality seems very simple, the modeling of heat diffusion coefficient κ (4.3) must be certificated. In other words, when we adopt different origin of turbulent suppression, the hysteresis condition may be represented differently. The hysteresis condition derived from our model (3.25) or (3.26) is universally approved. Looking at Fig. 4.5, top figure is the plot of η $(= 1/\kappa)$, bottom figure is for the relation between flux and temperature gradient. The sharp increase of η is exhibited as the cause of hysteresis.

The power lamp experiment has been done to clarify the properties of hysteresis[28]. Figure 4.6 is the fitting of the equation (4.7) and arbitrary function satisfying equation(3.25). Here we assumed, for the latter, $a(T)$ of the equation (2.1) as arc tangent such as including rapidly increasing region. Since even this arbitrary function without any detailed mechanism can be

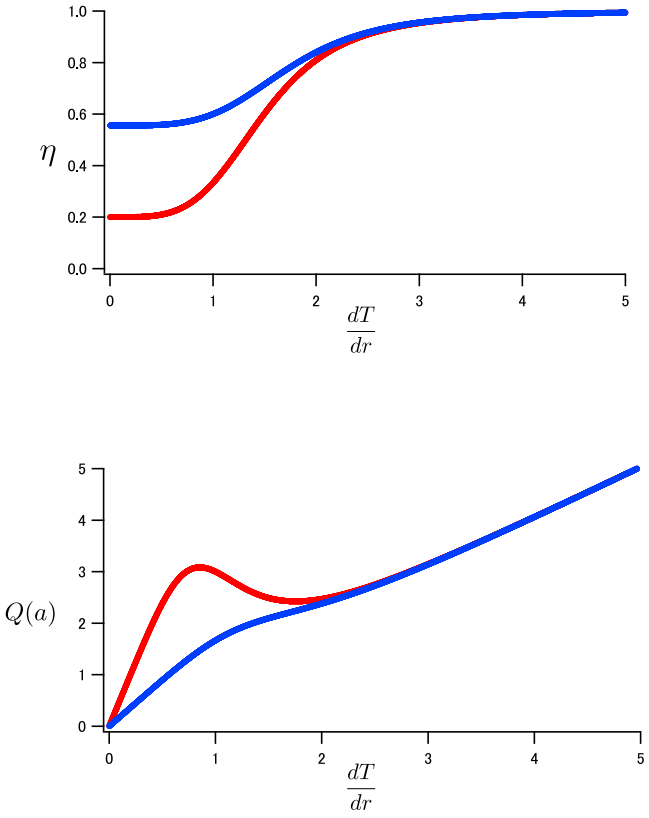

Figure 4.5: Top : Plot of η. Bottom : Plot of $Q(a)$ as a function of temperature. The colors of lines are homologized.

fitted well, the thermodynamic condition of hysteresis (3.25) is thought to be critical condition. There are other models of the mechanism of hysteresis; for example, the power of the denominator in equation (4.7) is two[28]. In any case, the condition (3.25) is a mutual condition of hysteresis.

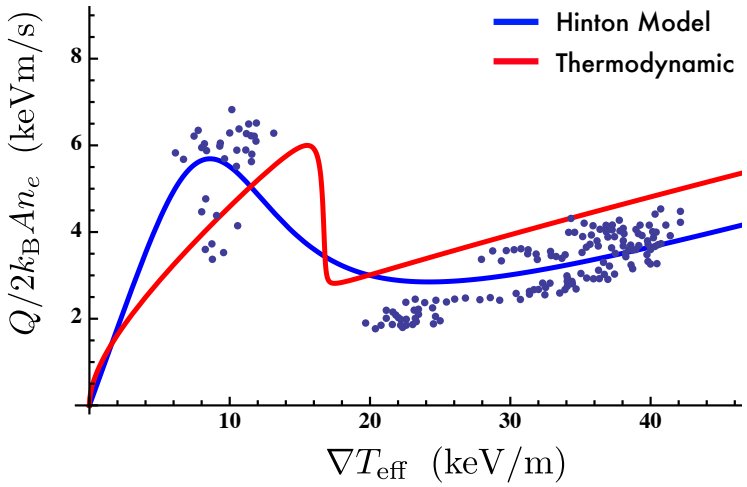

Figure 4.6: Experimental data in Alcator C-Mod. Blue: Fitted by equation (4.7). Red: Fitted by the arbitrary function satisfying equation(3.25) (here we use arc tangent).

Now we remember the discussion of parameter dependence of impedance in Sec. 3.3. Equation (4.8) is applied as the tangible parameterization. How the $F-T$ diagram depends on the parameters (κ_n, κ_a and λ_a) is speculated.

Embedding Δr into the parameters, we define $K_n \equiv \kappa_n/\Delta r$, $K_a \equiv \kappa_n/\Delta a$ and $\Lambda_a \equiv \lambda_a/(\Delta r)^4$. Then equation (4.8) is rewritten as,

$$\left(K_n + \frac{K_a}{1 + \Lambda_a (T - T_0)^4}\right)(T - T_0) = F \tag{4.10}$$

With two critical point $(T_1^{\mathrm{c}},\ F(T_1^{\mathrm{c}}))$ and $(T_2^{\mathrm{c}},\ F(T_2^{\mathrm{c}}))$, we approximately evaluate the area of hysteresis as,

$$(T_2^{\mathrm{c}} - T_1^{\mathrm{c}})(F(T_1^{\mathrm{c}}) - F(T_2^{\mathrm{c}})) \tag{4.11}$$

as shown in Fig. 4.7. Thought this is rough approximation, the rigorous area, at least, tends to be large as the approximated area becomes large.

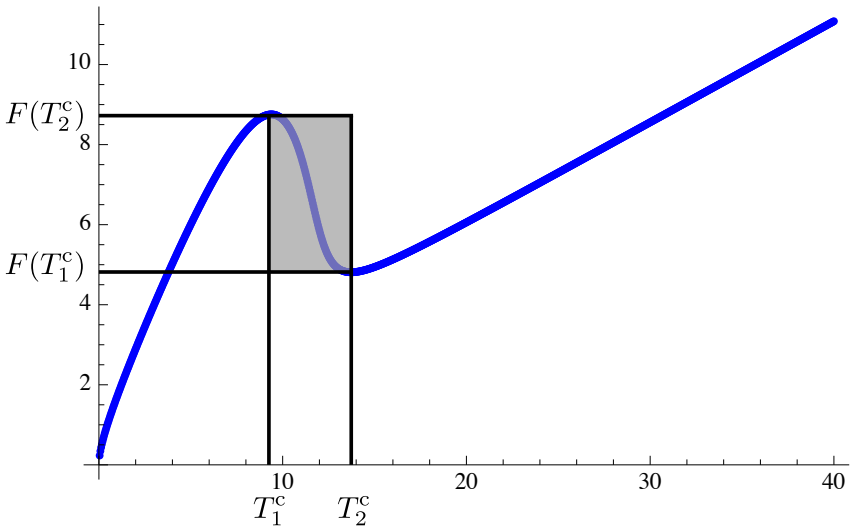

Figure 4.7: The approximated area of hysteresis loop

The critical points are calculated as,

$$
\begin{aligned}
T_1^{\mathrm{c}} &= \left(-\frac{1}{\Lambda_a}+\frac{3K_a}{2K_n\Lambda_a}+\frac{\sqrt{K_a(9K_a-16K_n)}}{2K_n\Lambda_a}\right)^{1/4} \\
T_2^{\mathrm{c}} &= \left(-\frac{1}{\Lambda_a}+\frac{3K_a}{2K_n\Lambda_a}-\frac{\sqrt{K_a(9K_a-16K_n)}}{2K_n\Lambda_a}\right)^{1/4} \\
F(T_1^{\mathrm{c}}) &= \left(-\frac{1}{\Lambda_a}+\frac{3K_a}{2K_n\Lambda_a}-\frac{\sqrt{K_a(9K_a-16K_n)}}{2K_n\Lambda_a}\right)^{1/4}\left(K_n+\frac{K_a}{1+\left(-\frac{1}{\Lambda_a}+\frac{3K_a}{2K_n\Lambda_a}-\frac{\sqrt{K_a(9K_a-16K_n)}}{2K_n\Lambda_a}\right)\Lambda_a}\right) \\
F(T_2^{\mathrm{c}}) &= \left(-\frac{1}{\Lambda_a}+\frac{3K_a}{2K_n\Lambda_a}+\frac{\sqrt{K_a(9K_a-16K_n)}}{2K_n\Lambda_a}\right)^{1/4}\left(K_n+\frac{K_a}{1+\left(-\frac{1}{\Lambda_a}+\frac{3K_a}{2K_n\Lambda_a}+\frac{\sqrt{K_a(9K_a-16K_n)}}{2K_n\Lambda_a}\right)\Lambda_a}\right)
\end{aligned}
$$

Then we define $M \equiv Ka/Kn \quad (> 16/9)$. T_1^{c} is plotted on Fig. 4.8; The bifurcation temperature increases when Λ_a is small or M is large.

The area of the loop is plotted on Fig. 4.9. It is obvious that the area is large where T_1^{c} is large. In other word, such a system that resist a bifurcation finally bifurcates to a further state (amassed the input energy).

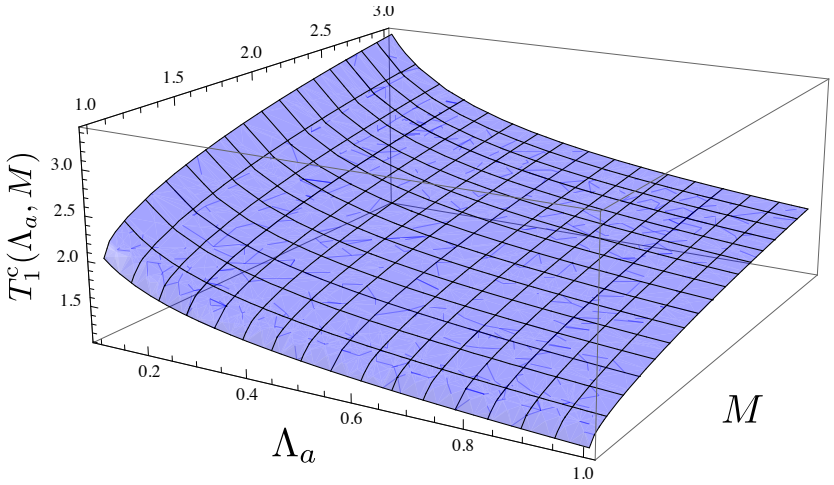

Figure 4.8: Plot of T_1^c as a function of Λ and M.

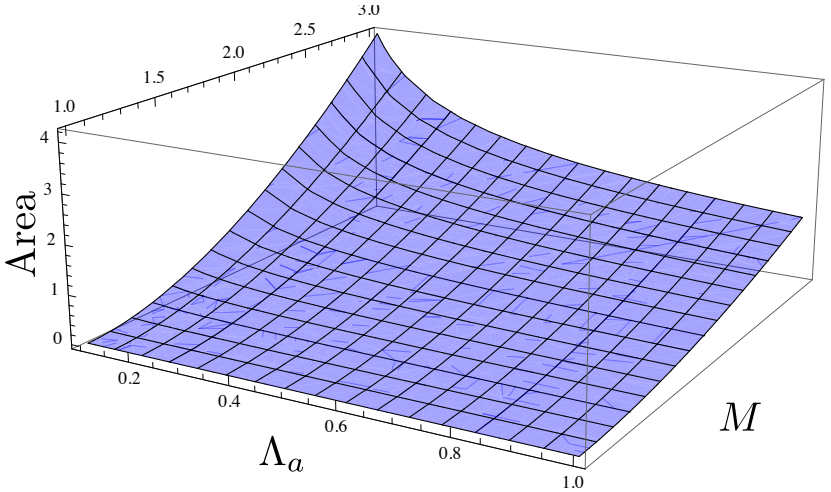

Figure 4.9: Plot of the area of hysteresis loop as a function of Λ_a and M.

Chapter 5

Conclusion

The bifurcation and hysteresis phenomena in a turbulent system (we consider H-mode as a typical example) is analyzed by using the phenomenological model at turbulent boundary layer. The stability of multiple solutions (linear solution and nonlinear solution) proves that solution bifurcate to nonlinear solution whichever the independent variable F or T we select. The thermodynamic function $\Phi(\beta, F)$ is introduced and used as beneficial tool to analyze the heat engine model. We encounter entropy production rate as a part of the thermodynamic function. While an entropy production rate determined from fluid dynamics comes to complicated form in the nonlinear state with flow, we obtain the entropy production rate from thermodynamic laws that suitable for

analyzing even in nonlinear state.

The operation point of the model appears not on a critical point of entropy production rate but of the thermodynamic function $\Phi(\beta, F)$. Dual relation of entropy production rate, that controlling flux derives "maximum" and controlling temperature derives "minimum" by contraries, is also explained by the thermodynamic function. $\Phi(\beta, F)$ is obtained from manipulating Legendre transformation to entropy production $\dot{S}(\beta)$. $\Phi(\beta, F)$ can be interpreted as a mapping between the graph of $\dot{S}(\beta)$ and the family of tangents from the geometric interpretation of the Legendre transformation. The tangent line problem of the entropy production rate is the cause of reversal of mini-max. The process is shown in Fig. 3.4.

Next we exhibit a condition of hysteresis. A sharp increase of impedance η gives a folding structure to the relation between F and T (multiple solutions). It is also shown that the forward process and the backward process differ when the folding structure exists from thermodynamic stability. The threshold of hysteresis is (3.25) or (3.26). More general discussion is made by the thermodynamic function. The folding structure of the relation between F and T is rephrased as the inflection point of $S(\beta)$. The jump of the solution is characteristically appears in the tangent line problem (Fig. 3.9).

All above discussions is based only on thermodynamic laws. We take neoclassical theory as a example and verified the theory and our model join smoothly. In a thin layer, such that heat flux is assumed to be constant, temperature gradient is also assumed to be constant. The relation of temperature and flux, then, becomes concretization of our model. The condition of hysteresis is also substantiated and gives realistic threshold. The function that satisfies the bifurcation condition is fitted well to the experimental data of Alcator C-Mod. Since even a rough function is fitted well, the thermodynamic condition of hysteresis is mutual to various models of L-H transisiton. The diagram of temperature versus flux depends on the shape of the impedance; The algebraic relation is derived with the model of Hinton. An area of hysteresis loop is large when a critical temperature of bifurcation is large.

Appendix A

Derivation of entropy production rate

Extensive variable S, entropy, satisfies $S(\lambda U, \lambda V) = \lambda S(U, T)$. Differentiating this with respect to λ,

$$U\frac{\partial S}{\partial U} + V\frac{\partial S}{\partial V} = S. \tag{A.1}$$

Substituting Maxwell's relations,

$$Ts = u + Pv \tag{A.2}$$

is obtained. Lower case characters represent being normalized by total mass

M. Energy density is written as $e = u + |\boldsymbol{v}|^2/2$ where $\boldsymbol{v}$ is flow velocity. Multiplying mass density $\rho \equiv 1/v$ to equation (A.2),

$$T\rho s = \rho e - \rho\frac{|\boldsymbol{v}|^2}{2} + P \tag{A.3}$$

Differentiation of this equation is,

$$Td(\rho s) + \rho s dT = d(\rho e) - \frac{|\boldsymbol{v}|^2}{2} - \rho\boldsymbol{v}\cdot d\boldsymbol{v} + dP \tag{A.4}$$

Using Gibbs—Duhem equation $sdT = vdP$ without chemical potential,

$$d(\rho s) = \frac{1}{T}d(\rho e) - \frac{1}{T}\frac{|\boldsymbol{v}|^2}{2}d\rho - \frac{1}{T}\rho\boldsymbol{v}\cdot d\boldsymbol{v} \tag{A.5}$$

Finally we obtain the equation of differentiation of entropy density.

$$\frac{\partial}{\partial t}(\rho s) = \frac{1}{T}\frac{\partial}{\partial t}(\rho e) - \frac{\boldsymbol{v}}{T}\cdot\frac{\partial}{\partial t}(\rho\boldsymbol{v}) + \frac{1}{T}\frac{|\boldsymbol{v}|^2}{2}\frac{\partial\rho}{\partial t} \tag{A.6}$$

Energy conservation law is written with pressure tensor P, stress tensor Π and heat flow $\boldsymbol{f}$.

$$\frac{\partial}{\partial t}(\rho e) + \nabla\cdot[\rho e\boldsymbol{v} + (P+\Pi):\boldsymbol{v} + \boldsymbol{f}] = 0 \tag{A.7}$$

Mass conservation law is written as,

$$\frac{\partial \rho}{\partial t} + \nabla \cdot (\rho \boldsymbol{v}) = 0 \tag{A.8}$$

Substituting equation (A.7) and (A.8) into equation (A.6), we can obtain following equation.

$$\frac{\partial}{\partial t}(\rho s) + \nabla \cdot \boldsymbol{j}_s = \sigma[s] \tag{A.9}$$

Where $\boldsymbol{j_s}$ denotes entropy flux and $\sigma[s]$ denotes entropy production.

$$\boldsymbol{j}_s \equiv \rho s \boldsymbol{v} + \frac{\boldsymbol{f}}{T}$$

$$\sigma[s] \equiv (\boldsymbol{f} + \Pi : \boldsymbol{v}) \cdot \nabla \left(\frac{1}{T}\right) + \Pi : \nabla \left(-\frac{\boldsymbol{v}}{T}\right) \tag{A.10}$$

The first and second term of $\boldsymbol{j_s}$ equals advection of entropy by heat flow and mass flow respectively. When mass flow $\boldsymbol{f}$ equals zero, the local entropy production rate is simply represented as $\boldsymbol{f} \cdot \nabla(1/T)$.

Appendix B

Legendre transformation as tangent line problem

Legendre transformation is a popular technique some times seen in equilibrium thermodynamics. From the mathematical point of view, this transformation means exchange of independent variable and dependent variable. Graphically tangent line problem is also equivalent to Legendre transformation.

From the first law of thermodynamics,

$$dU = \frac{\partial U}{\partial S} dS + \frac{\partial U}{\partial V} dV = TdS - pdV \tag{B.1}$$

Internal energy $U = U(S, T)$ is then the function of S and T. Helmholtz

free energy is defined as,

$$F = U - TS \tag{B.2}$$

$$dF = \left(\frac{\partial U}{\partial S} - T\right) dS - SdT + \frac{\partial U}{\partial V} dV \tag{B.3}$$

From equation (B.1),

$$\frac{\partial F}{\partial S} = \frac{\partial U}{\partial S} - T = 0 \tag{B.4}$$

Under this condition, equation (B.3) is rewritten as $dF = -SdT - pdV$. Therefore $U(S,T)$ is transformed to $F(V,T)$. Equation (B.4) means that F is defined on the ridge line of S.

$$F = \inf(U - TS) \tag{B.5}$$

Graphical understanding is show by Fig. B.1. When U is convex downward, infimum is uniquely determined. (If U is convex upward by contraries, supremum is uniquely determined.) In either case, determined point is tangent point where the inclination is F. Other important thermodynamic variables, enthalpy or Gibbs free energy, are derived from Legendre transformation.

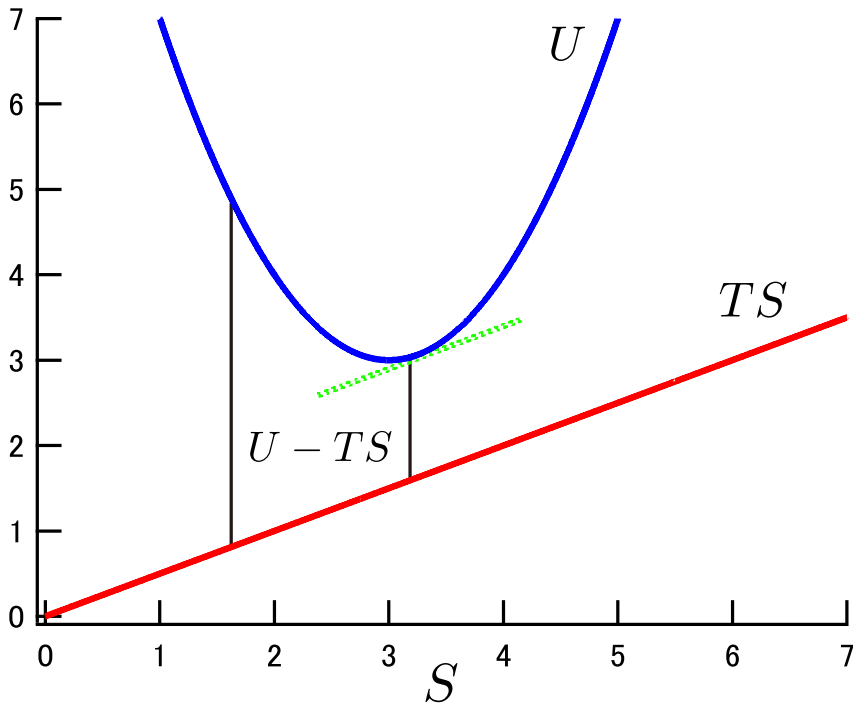

Figure B.1: If U is convex downward, translation is given on the point that gives infimum of the distance of two curves (tangent point), uniquely determined.

References

[1] G.K. Vallis and M.E. Maltrud, J. Phys. Oceanogr. 23, 1346 (1993).

[2] P. H. Diamond, S-I. Itoh, K. Itoh. and T. S. Hahm, Plasma Phys. Control. Fusion 47 (2005) R35—R161.

[3] http://folk.uio.no/gardini/sun.html,

http://www.pppl.gov/ hammett/collaborators/mbeer/

[4] G. Nicolis and I. Prigogine, Self-Organization in Nonequilibrium Systems —From Dissipative Structures to Order through Fluctuations (Wiley, New York, 1977).

[5] G. W. Paltridge, Q. J. R. Meteorol. Soc. 101, 475 (1975); G. W. Paltridge, Nature (London) 279, 630 (1979).

[6] P. H. Wyant, A. Mongroo, and S. Hameed, J. Atmos. Sci. 45, 189 (1988).

[7] H. Grassl, Q. J. R. Meteorol. Soc. 107, 153 (1990).

[8] S. Shimozawa and H. Ozawa, Q. J. R. Meteorol. Soc. 128, 2115 (2002).

[9] R. D. Lorenz, J. I. Lunine, and P. G. Withers, Geophys. Res. Lett. 28, 415, DOI: 10.1029/2000GL012336 (2001).

[10] H. Ozawa, S. Shimokawa, and H. Sakuma, Phys. Rev. E 64, 026303 (2001).

[11] R. Dewar, J. Phys. A 36, 631 2003.

[12] R. Dewar, J. Phys. A: Math. Gen. 38 (2005) L371.

[13] Z. Yoshida, S. M. Mahajan, Phys. Plasmas 15, 032307 (2008).

[14] 非平衡系の統計力学，北原和夫，岩波書店.

[15] 非平衡系の科学，北原和夫，吉川研一，講談社サイエンティフィク.

[16] F. Wagner, *et al.*, Phys. Rev. Lett. 49, 1408 (1982).

[17] ASDEX Team, 1989, Nucl. Fusion 29, 1959.

[18] V. Erckmann et al., Phys. Rev. Lett. 70, 2086 (1993).

[19] Ryter F et al 1993 Controlled Fusion and Plasma Physics, Proc. 20th Euro. Conf. (Lisbon) vol 17C, part I (Geneva: European Physical Society) p 23.

[20] K. Itoh and S.-I. Itoh, Plasma Phys. Controlled Fusion 38, 1 (1996).

[21] K. H. Burrell et al., Plasma Phys. 4, 1499 (1997).

[22] P. W. Terry, Rev. Mod. Phys. 72, 1 (2000).

[23] F. L. Hinton, Phys. Fluids B 3, 696 (1990).

[24] F. L. Hinton, G. M. Staebler, Phys. Fluids B 5, (1993), 1281.

[25] H. Biglari, P. H. Diamond, and P. W. Terry, Phys. Fluids B2, 1 (1990).

[26] R. J. Groebner, K. H. Burrell and R. P. Seraydarian, Phys. Rev. Lett. 64, 3015 (1990).

[27] F.L. Hinton and R.D. Hazeltine, Rev. Mod. Phys. 48, 239 (1976); S.P. Hirshman and D.J. Sigmar, Nucl. Fusion 21, 1079 (1981).

[28] A. E. Hubbard et al.Plasma Phys. Control. Fusion 44 (2002) A359—A366

Acknowledgements

I would like to show my best appreciation to Professor Zensho Yoshida for the great coaching. I enjoyed a lot of knowledge and way of thinking of science. He might have had difficulty teaching me because I had little knowledge about mathematics and physics. His earnest teaching stimulated greatly and let me have a deep interest. This research owes a lot to his suggestion. On the discussions, he carefully told me what was insufficient and what should I have studied to solve it. On the presentation, my inadequate skill of presentation was pointed out. As a result, I got to understand the genuine background of my research.

I also would like to thank Associate Professor Masaru Furukawa. He sometimes advised me of mathematical techniques in this research. Above all, his lecture of fusion plasma stimulated me a lot. Once, I had have little interest in fusion science. However after his lecture, I got an interest and motivated.

I also want to thank Assistant Professor Haruhiko Saito. Though I have few occasion to discuss about science, his well-organized effort of research, such as coming to laboratory earlier than anyone and going back later than anyone, raised my consciousness. I want to thank Mr. Junji Morikawa to spend joyful lunch time with.

I am also grateful to students in our laboratory. Firstly Mr. Yano kindly told me various things from campus life to plasma science. Student seminar with Mr. Numazawa made me have basics of theories of turbulence. Advice about β model from Mr. Harima will help me anytime soon. I am sorry to junior students, Mr. Emoto, Mr. Kobayashi and Mr. Sugiura, that I could not help their work. Mr. Vogel corrected my English of thesis. And my skill of talking English was greatly educated due to him. Senior students, Mr. Hayashi and Ms. Nakatsu, delighted my first year of graduate school. Contemporary members, Mr. Mizushima and Mr. Tadachi, work hard and learn from each other with me.

I also would like to show my appreciation to Ms. Kitayama for her encourgement and kindness. I could spend joyful time in parties with members of Ogawa laboratory.

Finally I want to give my thanks to my family supporting my life.

研究発表

1. 川面洋平，吉田善章，プラズマの乱流熱輸送におけるヒステリシスの数理解析，日本物理学会第 64 回年次大会，27pSP-12，2009 年 3 月於立教大学

2. 川面洋平，吉田善章，Flux driven 系のエントロピー生成率に関する変分と安定性，日本流体力学会 年会 2009，2009 年 9 月於東洋大学

3. 川面洋平，吉田善章，Flux driven 系のエントロピー生成率に関する変分と安定性，日本物理学会第 65 回年次大会，28aQC-9，2009 年 9 月於熊本大学

4. 川面洋平，吉田善章，乱流境界層の現象論モデルとエントロピー生成率，日本物理学会第 66 回年次大会，21pEJ-6，2010 年 3 月於岡山大学（予定）